Doctoral Dissertation

Study on the Effect of Chemical Structures of Photo-Responsive Non-Nucleoside Triphosphates on the Interaction with Motor Proteins

（光応答性非ヌクレオシド三リン酸の化学構造がモータータンパク質との相互作用に与える影響に関する研究）

Md. Jahirul Islam

Graduate School of Life Science, Hokkaido University

March 2019

Declaration

I hereby declare that the matter embodied in this thesis entitled "Study on the Effect of Chemical Structures of Photo-Responsive Non-Nucleoside Triphosphates on the Interaction with Motor Proteins" is the result of investigations carried out by me under the supervision of ***Prof. Nobuyuki Tamaoki*** at the Laboratory of Smart molecules, Transdisciplinary Life Science Course, Graduate School of Life Science, Hokkaido University, Japan and it has not been submitted elsewhere for the award of any degree or diploma.

In keeping with the general practice of reporting scientific observations, due acknowledgement has been made whenever the work described has been based on the findings of the other investigators. Any omission that might have occurred by oversight or error of judgments is regretted.

Md. Jahirul Islam

Certificate

I hereby certify that the work described in this thesis entitle "Study on the Effect of Chemical Structures of Photo-Responsive Non-Nucleoside Triphosphates on the Interaction with Motor Proteins" has been carried out by ***Md. Jahirul Islam***, under my supervision at the Laboratory of Smart Molecules, Transdisciplinary Life Science Course, Graduate School of Life Science, Hokkaido University, Japan

Prof. Nobuyuki Tamaoki

(Research Supervisor)

Table of contents

Chapter 1.

General introduction

1.1. Background and aim of this thesis

Molecular motor proteins including the linear and rotary motors are mechanical enzymes that can move by catalytically converting chemical energy of adenosine triphosphate (ATP) into mechanical work[1-3]. Especially, cytoskeletal motor proteins including conventional kinesin-1[4,5] and myosin II[6,7] that can move unidirectionally along their associated cytoskeletal filaments are pivotal for maintaining the cellular functions. Kinesin-1 mainly conducts the intracellular active transport of organelles and macromolecular assemblies along microtubules from the cell center towards cell periphery (i.e. anterograde transport). Myosin II moving along actin filaments toward the barbed end is a leading contributor to muscle contraction and cell migration. In spite of the different associated filaments, these two biomolecular motors possess similar engines using ATP to generate the mechanical force. Due to this immense potential of producing force with nano-sized motors, numerous attempts have been made to develop the functional nano-devices[8,9].

Gliding motility assay is the well-established model system to study and engineer the bio-molecular motors *in vitro*[4,10]. In this versatile approach, the gliding motility of fluorescently labeled microtubules or actin filaments driven by bio-motors (kinesin or myosin) which are bound to the glass surface can be visualized with fluorescence microcopy. To develop the controllable nano-devices using bio-molecular motors, various external stimuli including electricity[11-13], heat[14-21], light[22-27] and so on have been applied. In particular, photo-controllable approaches should be drawing the center of attention due to the high spatiotemporal operability and high switchability. For instance, Higuchi *et al*.[22] and Hess *et al*.[23] demonstrated caged ATP (photolabile protected ATP)

as the photocontrolled one-way switch that was from motility OFF to ON using ultraviolet light. In addition to these excellent methods, our group recently reported the reversibly photocontrollable ATP analogues, i.e. non-nucleoside triphosphate molecules based on azobenzene (AzoTPs), for kinesin-1[28] and myosin II[29]. AzoTPs in *trans* state of their azobenzene moiety can be recognized as the enzyme substrate for both of kinesin and myosin as well as natural energy molecule ATP for powering the motor proteins, whereas they in *cis* state cannot be recognized. However, the AzoTPs substrate specificity in molecular motors and the mechanism of substrate recognition and their photoreversibility remain unclear. And the inhibitory behavior of non-hydrolysable derivatives of AzoTPs in actin-myosin and microtubules-kinesin *in vitro* motility assays was unknown.

In this thesis, the author intended to develop motor specific photo-responsive azo-triphosphate based substrate for motor protein and mechanistic insight of the substrate recognition by motor proteins and photoreversibility. The author also intended to explore the photo-responsive inhibitory behavior of AzoTP based non-hydrolysable triphosphate molecules in the actin-myosin and microtubules-kinesin *in vitro* motility assay.

In chapter 2, The author describes several azobenzene-tethered triphosphates to photoreversibly drive kinesin and myosin in microtubules-kinesin and actin-myosin in vitro motility assays. Through the motility assays, the myosin-selective photo-responsive substrate is successfully discovered. Using this substrate, the myosin motility is selectively photomanipulated in the kinesin-myosin composite motility assay, while it shows almost no kinesin motility. This mechanistic insight of driving myosin selectively with photoswitchability is explained through the docking simulation study.

In chapter 3, The author describes several azobenzene-tethered non-hydrolysable tri-phosphate molecules to investigate their photo-responsive inhibitory behavior in microtubules-kinesin and actin-myosin in vitro motility assays. The non-hydrolysable tri-phosphate molecules works as photo-responsive inhibitor in the motor protein systems whose inhibitory behavior is reversibly regulated by *cis-trans* isomerization.

In chapter 4, conclusions of the thesis are shown.

1.2. References

1 R. D. Vale and R. A. Milligan, *Science*, 2000, **288**, 88–95.

2 M. Yoshida, E. Muneyuki and T. Hisabori, *Nat. Rev. Mol. Cell Biol.*, 2001, **2**, 669–677.

3 M. Schliwa, *Molecular motors*, Wiley-VCH Verlag GmbH & Co. KGaA, Weinheim, Germany, 2003.

4 R. D. Vale, T. S. Reese and M. P. Sheetz, *Cell*, 1985, **42**, 39–50.

5 J. Howard, *Annu. Rev. Physiol.*, 1996, **58**, 703–729.

6 V. Mermall, P. L. Post, M. S. Mooseker, *Science,* 1998, **279**, 527–533.

7 S. J. Kron and J. A. Spudich, *Proc. Natl. Acad. Sci. U. S. A.*, 1986, **83**, 6272–6276.

8 A. Goel and V. Vogel, *Nat. Nanotechnol.*, 2008, **3**, 465–475

9 S. Aoyama, M. Shimoike and Y. Hiratsuka, *Proc. Natl. Acad. Sci. U. S. A.*, 2013, **110**, 16408–16413.

10 S. J. Kron and J. a Spudich, *Proc. Natl. Acad. Sci. U. S. A.*, 1986, **83**, 6272–6276.

11 M. G. L. van den Heuvel, M. P. de Graaff, C. Dekker, *Science*, 2006, **312**, 910–914.

12 M. Uppalapati, Y. M. Huang, T. N. Jackson and W. O. Hancock, *Small*, 2008, **4**, 1371–1381.

13 E. Kim, K. E. Byun, D. S. Choi, D. J. Lee, D. H. Cho, B. Y. Lee, H. Yang, J. Heo, H. J. Chung, S. Seo and S. Hong, *Nanotechnology*, 2013, **24**, 195102–195107.

14 H. Kato, E. Muto, T. Nishizaka, T. Iga, K. Kinosita JR and S. Ishiwata, *Proc. Natl. Acad. Sci. U. S. A.*, 1999, **96**, 9602–9606.

15 G. Mihajlović, N. M. Brunet, J. Trbović, P. Xiong, S. von Molnár, and P. B. Chase, *Appl. Phy. Lett.*, 2004, **85**, 1060–1062.

16 L. Ionov, M. Stamm and S. Diez, *Nano Lett.*, 2006, **6**, 1982–1987.

17 F. Wang, N. M. Brunet, J. R. Grubich, E. A. Bienkiewicz, T. M. Asbury, L. A. Compton, G. Mihajlović, V. F. Miller and P. B. Chase, *J. Biomed. Biotechnol.*, 2011, **2011**, 435271.

18 T. Korten, W. Birnbaum, D. Kuckling and S. Diez, *Nano Lett.*, 2012, **12**, 348–353.

19 N. M. Brunet, G. Mihajlović, K. Aledealat, F. Wang, P. Xiong, S. von Molnár and P. B. Chase, *J. Biomed. Biotechnol.*, 2012, **2012**, 657523.

20 C. Reuther, R. Tucker, L. Ionov and S. Diez, *Nano Lett.*, 2014, **14**, 4050–4057.

21 N. M. Brunet, P. B. Chase, G. Mihajlović and B. Schoffstall, *Arch. Biochem. Biophys.*, 2014, **552-553**, 11-20.

22 H. Higuchi, E. Muto, Y. Inoue and T. Yanagida, *Proc. Natl. Acad. Sci. U. S. A.*, 1997, **94**, 4395–4400.

23 H. Hess, J. Clemmens, D. Qin, J. Howard and V. Vogel, *Nano Lett.*, 2001, **1**, 235–239.

24 R. Tucker, P. Katira and H. Hess, *Nano Lett.*, 2008, **8**, 221–226.

25 K. R. S. Kumar, T. Kamei, T. Fukaminato and N. Tamaoki, *ACS Nano*, 2014, **8**, 4157–4165.

26 K. R. S. Kumar, A. S. Amrutha and N. Tamaoki, *Lab Chip*, 2016, **16**, 4702–4709.

27 A. S. Amrutha, K. R. S. Kumar, T. Kikukawa and N. Tamaoki, *ACS Nano*, 2017, **11**, 12292–12301.

28 N. Perur, M. Yahara, T. Kamei and N. Tamaoki, *Chem. Commun.*, 2013, **49**, 9935–9937.

29 H. M. Menezes, M. J. Islam, M. Takahashi and N. Tamaoki, *Org. Biomol. Chem.*, 2017, **15**, 8894–8903.

Chapter 2.

Substrate selectivity and its mechanistic insight of the photo-responsive non-nucleoside triphosphate for myosin and kinesin

2.1. Introduction

In the bottom-up approach to build up the functional nano-system, bio-molecular motors including kinesin and myosin should be attractive biomaterials. To afford the precise controllability to the nano-system based on bio-molecular motors, photo-controlled techniques have been drawing the center of attention due to high spatiotemporal operability and high switchability. Photo-reversible energy molecule AzoTPs in *trans* state of their azobenzene moiety can be recognized as the enzyme substrate for both of kinesin and myosin as well as natural energy molecule ATP for powering the motor proteins, whereas they in *cis* state cannot be recognized[1,2].

Due to the well-conserved engine mechanism in kinesin and myosin[3], ATP can efficiently power each of kinesin and myosin. In sharp contrast, other nucleotides including synthetic ATP analogues exhibited the unique specificity towards kinesin and/or myosin[4-13]. The specific substrate should be a useful tool for analyzing which proteins are responsible for the motor-based motility in a crude system. Herein, the author describe the successful discovery of the myosin-selective photoswitchable energy molecule. Through the structure-activity relationship study in both of microtubule-kinesin and actin-myosin system, the author found the myosin-selective AzoTP derivative (**1e**) with hydrophobic bulky substitution on the azobenzene moiety retaining high photoswitchabiity, which was also demonstrated in the kinesin-myosin composite system[14]. Compared with ATP as a standard substrate, **1e** exhibited the 9.4-fold higher selectivity toward actin-myosin system than microtubule-kinesin system. This selectivity mechanism was rationally explained through the docking simulation study.

2.2. Results and discussion

2.2.1. Synthesis and photo-responsive behavior of AzoTP molecules

To investigate the photo-reversible powering properties of AzoTP molecules toward kinesin and myosin, the author synthesized five AzoTP molecules, **1a**-**1e** (Fig 2.1) with different types of linkages and azobenzene substitutes. These AzoTP molecules were designed to compare the length and flexibility of linkers in ethyl (**1b**), propyl (**1c**) and ethyl ether linkages (**1d**) with the original acetamide linker in **1a** and the steric and hydrophobic effects of 3'- and 4'-methyl groups on an azobenzene ring in **1e**. Photo-responsive AzoTP molecules can undergo reversible *cis-trans* isomerization by absorbing ultraviolet (UV) and visible (VIS) light, respectively (Fig. 2.1).

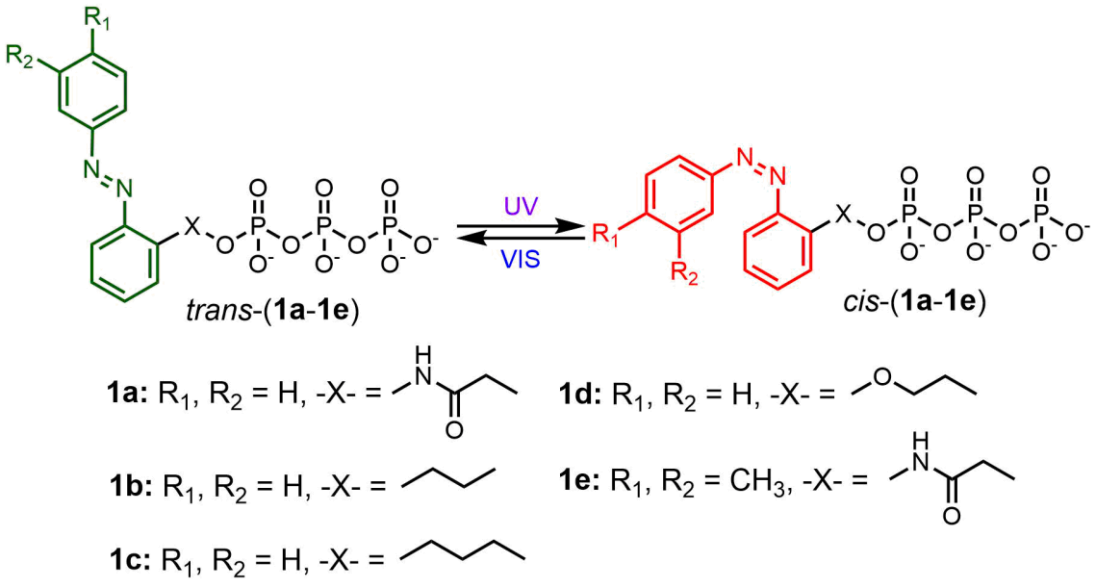

Fig. 2.1 Schematic representation of *cis-trans* photo isomerization of **1a**-**1e** with UV and VIS light irradiation.

UV-VIS absorption spectra of **1a**-**1e** in BRB-80 buffer before irradiation (BI) and after UV (365 nm) or VIS (436 nm) irradiation were shown in Fig. 2.2.

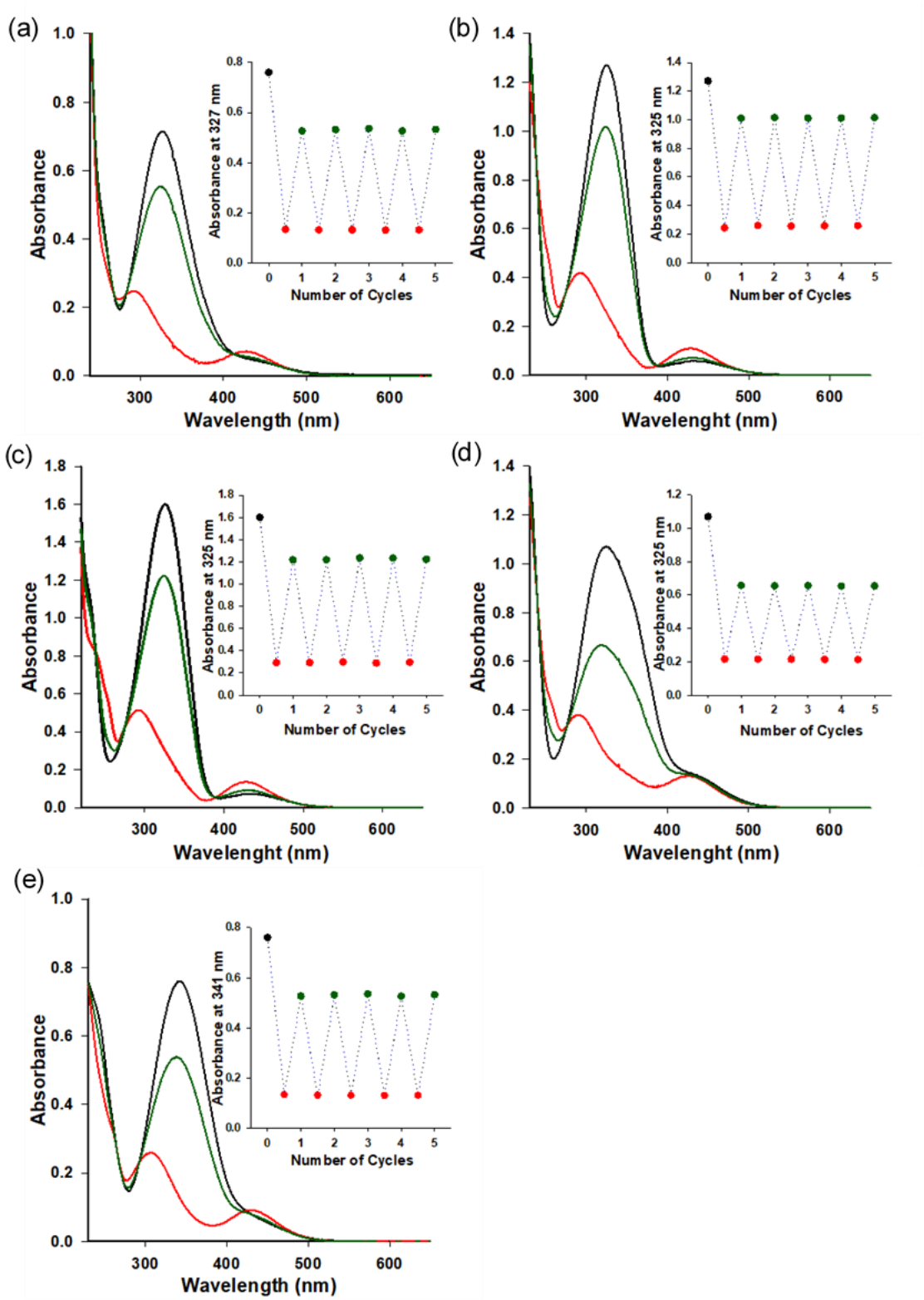

Fig. 2.2 UV-VIS absorption spectra of **1a**-**1e** before irradiation and in UV photostationary state (PSS) and VIS PSS. UV-VIS absorption spectra of (a) **1a** (4.4×10^{-4} M), (b) **1b** (8.9×10^{-4} M), (c) **1c** (9.5×10^{-4} M), (d) **1d** (7.1×10^{-4} M)

and (e) **1e** (5.2×10^{-4} M) in BRB-80 buffer at 25 °C. Before irradiation (black line), UV PSS (red line), VIS PSS (dark green line). Insets: Absorbance changes after the alternate irradiations with UV (20 sec) and VIS (150 sec) light for 5 cycles.

By the illumination of UV light to form *cis* rich states of AzoTPs (UV photostationary state, UV PSS), the π-π* band at around 327 nm in absorbance spectra decreased, while the n-π* band at around 430 nm increased. The opposite trend (namely, the increment of the π-π* band and the decrement of n-π* band) was observed by applying VIS light to reach the *trans* rich states (VIS PSS). The *cis*-*trans* isomer ratio of **1a**-**1e** at UV PSS and VIS PSS was calculated by ^{1}H NMR measurements as shown in Table 2.1 and Fig. 2.3.

Table 2.1. Ratio of *cis* and *trans* isomers at the UV and VIS PSS

AzoTP molecules	UV PSS		VIS PSS	
	cis (%)	*trans* (%)	*cis* (%)	*trans* (%)
1a	92	8	38	62
1b	87	13	25	75
1c	88	12	26	74
1d	93	7	50	50
1e	93	7	35	65

The author determined the *cis*-to-*trans* isomer ratio of **1a**, **1b**, **1d**, and **1e** using ^{1}H NMR spectroscopy previously.[1,2]

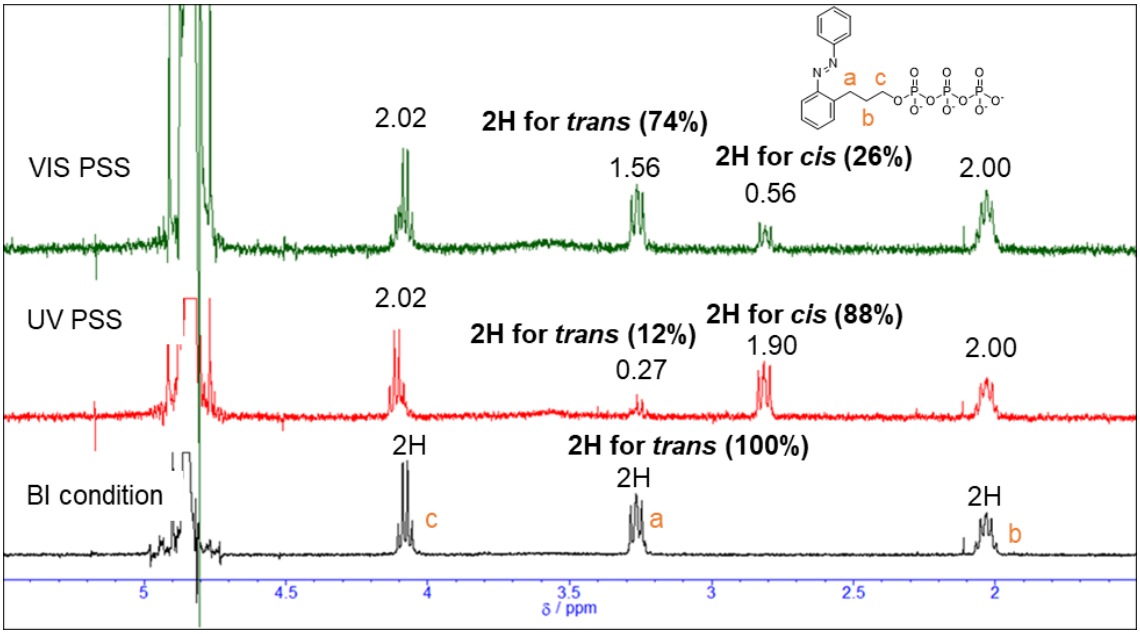

Fig. 2.3 Estimation of *cis*-to-*trans* ratio of **1c** at UV and VIS PSS. ^{1}H NMR spectra of **1c** in D_2O prior to irradiation and after irradiation with the UV and VIS light (at PSS condition). The area for methylene protons of **1c** at 3.27 ppm was studied at before irradiation (BI) condition; after irradiation with UV (PSS); and after irradiation with VIS (PSS). At UV PSS, *cis* to *trans* ratio was 88 : 12 and at VIS PSS, *cis* to *trans* ratio was 26 : 74.

The reversible photoisomerization of **1a**-**1e** could be recycled several times by alternating UV and VIS light irradiation without any fatigues. *cis* isomers of all AzoTPs shown here were stable in BRB-80 buffer at 25 ºC ($t_{1/2}$ > 3 days) enough to show insignificant thermal back reaction during the motility experiments (Fig. 2.4).

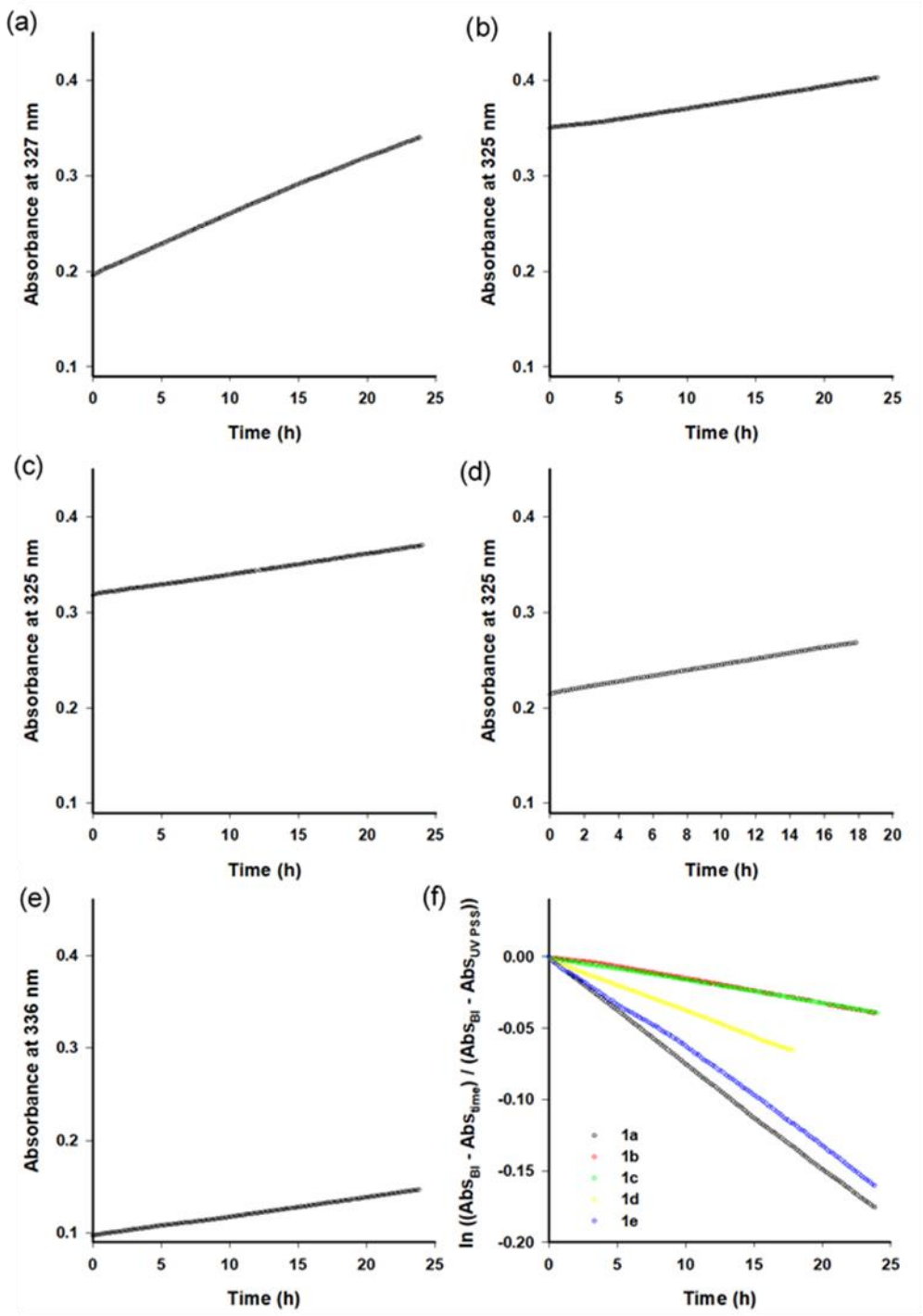

Fig. 2.4 Time course of the absorbance of (a) ***1a*** at 327 nm, (b) ***1b*** *at 325 nm*, (c) ***1c*** *at 325 nm*, (d) ***1d*** *at 325 nm*, (e) ***1e*** *at 336 nm* in BRB-80 buffer (pH 6.9) after UV irradiation and then incubated under dark condition at 25 °C. Conditions: [**1a**] = 6.8×10^{-4} M, [**1b**] = 12.1×10^{-4} M, [**1c**] = 10.0×10^{-4} M, [**1d**] = 7.1×10^{-4} M, [**1e**] = 3.0×10^{-4} M. (f) The plot for thermal isomerization rate determination of

1a-1e under dark condition at 25 °C; equation, $\ln\left(\frac{Abs\,(\mathrm{BI}) - Abs\,(\mathrm{time})}{Abs\,(\mathrm{BI}) - Abs\,(\mathrm{UV\ PSS})}\right) = -kt$ was used to determine the rate of the thermal isomerization reaction where *Abs* (BI), Absorbance at before irradiation; *Abs* (UV PSS), Absorbance at UV photo stationary state; *Abs* (time), Absorbance at different time interval in dark start from UV PSS. Rate constants, k = 0.0074 h^{-1} ($t_{1/2}$ = 94 h) for **1a**, k = 0.0016 h^{-1} ($t_{1/2}$ = 4.3 × 10^2 h) for **1b**, k = 0.0016 h^{-1} ($t_{1/2}$ = 4.3 × 10^2 h) for **1c**, k = 0.0037 h^{-1} ($t_{1/2}$ = 1.9 × 10^2 h) for **1d**, k = 0.0066 h^{-1} ($t_{1/2}$ = 1.1 × 10^2 h) for **1e**.

2.2.2. AzoTP molecules in actin-myosin *in vitro* motility assay

Very recently, we reported that AzoTPs **1a**, **1b**, **1d** and **1e** worked as photo-responsive myosin substrates on a photoreversible mode in actin-myosin gliding motility assay.[2] Table 2.2 summarizes the powering activity of **1a**, **1b**, **1d** and **1e** in actin-myosin gliding motility assay.

Table 2.2. Summary of AzoTP derivatives (**1a**, **1b**, **1d** and **1e**) in actin-myosin system

AzoTP derivatives/ATP	V_{max} (μm/s)	K_m (mM)	Gliding velocity switching* (%)
1a[2]	1.5 ± 0.04	0.10 ± 0.01	54
1b[2]	1.0 ± 0.1	0.18 ± 0.04	80
1d[2]	1.9 ± 0.2	0.091 ± 0.02	79
1e[2]	1.7 ± 0.2	0.27 ± 0.09	81

*Gliding velocity switching between *trans* and *cis*-rich state of AzoTP derivatives at saturated concentration, 1.0 mM for **1a** and **1e**; 0.50 mM for **1b** and **1d**.

The newly synthesized AzoTP **1c** was studied in the actin-myosin *in vitro* gliding motility assay (Fig. 2.5). AzoTP **1c** concentration dependent actin

filaments gliding velocity with reversible gliding velocity switching were shown in Fig. 2.5.

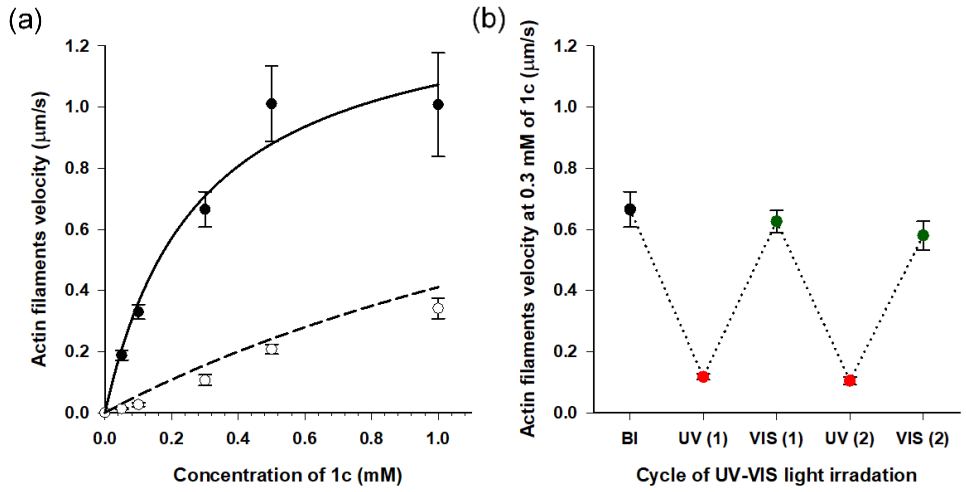

Fig. 2.5 Photoresponsive actin gliding motility with **1c** (a) Gliding velocity depending on the concentration of **1c**. (Filled circle (●): BI condition and open circle (○): after UV irradiation condition). Solid black line: curve fitting using the Michaelis-Menten equation (K_m = 0.28 ± 0.09 mM, V_{max} = 1.4 ± 0.2 μm/sec for **1c**) and dash black line: theoretical curve derived from solid black line for remaining *trans* isomer (12%) in *cis* rich state of **1c**. (b) Reversible photoregulation of the actin gliding velocity using **1c** (0.30 mM) with repeated UV and VIS light irradiation. Error bars represent the standard deviation of 10 actin filaments in a single flow cell.

The maximum gliding velocity (V_{max}) of actin filaments with **1c** was 1.4 μm/sec, which was 27% of V_{max} (5.1 μm/sec) compared with ATP. The gliding velocity of actin filaments was reversibly controlled for several cycles with repeated UV and VIS light illumination (Fig 2.5b). Similarly to other AzoTPs in actin-myosin system[2], the *cis* isomer of **1c** has no contribution to powering the myosin. The motility at UV PSS was originated from the remaining *trans* isomer

of **1c** (12%) as plotted the theoretical curves (dash black line in Fig. 2.5a). Therefore, the author concluded that in actin-myosin system, a wide range of AzoTP derivatives with different linkers and azobenzene moieties exhibited the myosin-powering activities in a photoswitchable mode.

2.2.3. AzoTP molecules in microtubule-kinesin *in vitro* motility assay

So far, only **1a**[1] was exploited in microtubule-kinesin *in vitro* motility assay in our previous study. Using **1a**, the microtubules gliding velocity was drastically photo-switched in concert with *cis*–*trans* photoisomerization of **1a** by illumination with two different wavelength of light (BI : 0.51 μm/sec, UV : 0.12 μm/sec at 3.0 mM). Encouraged by successful application of our AzoTPs to the actin-myosin system, the author investigated AzoTP derivatives, **1b**-**1e,** as the substrates of kinesin-1 to drive microtubules gliding in microtubule-kinesin system (Fig. 2.6, Table 2.3).

Table 2.3 Summary of AzoTP molecules in microtubule-kinesin system

AzoTP derivatives	V_{max} (μm/s)	K_m (mM)	Gliding velocity switching* (%)
1a[1]	0.83 ± 0.06	1.7 ± 0.2	76
1b	0.66 ± 0.02	0.82 ± 0.07	39
1c	0.60 ± 0.02	0.93 ± 0.09	26
1d	0.15 ± 0.03	1.0 ± 0.4	27
1e	0.058 ± 0.02	2.1 ± 1	N.D.

*Gliding velocity switching between *trans* and *cis*-rich states of AzoTP derivatives at saturated concentration, 3.0 mM for **1a**, **1b**, **1c** and **1d**; 2.0 mM for **1e**[15]. N.D. : Not Determined.

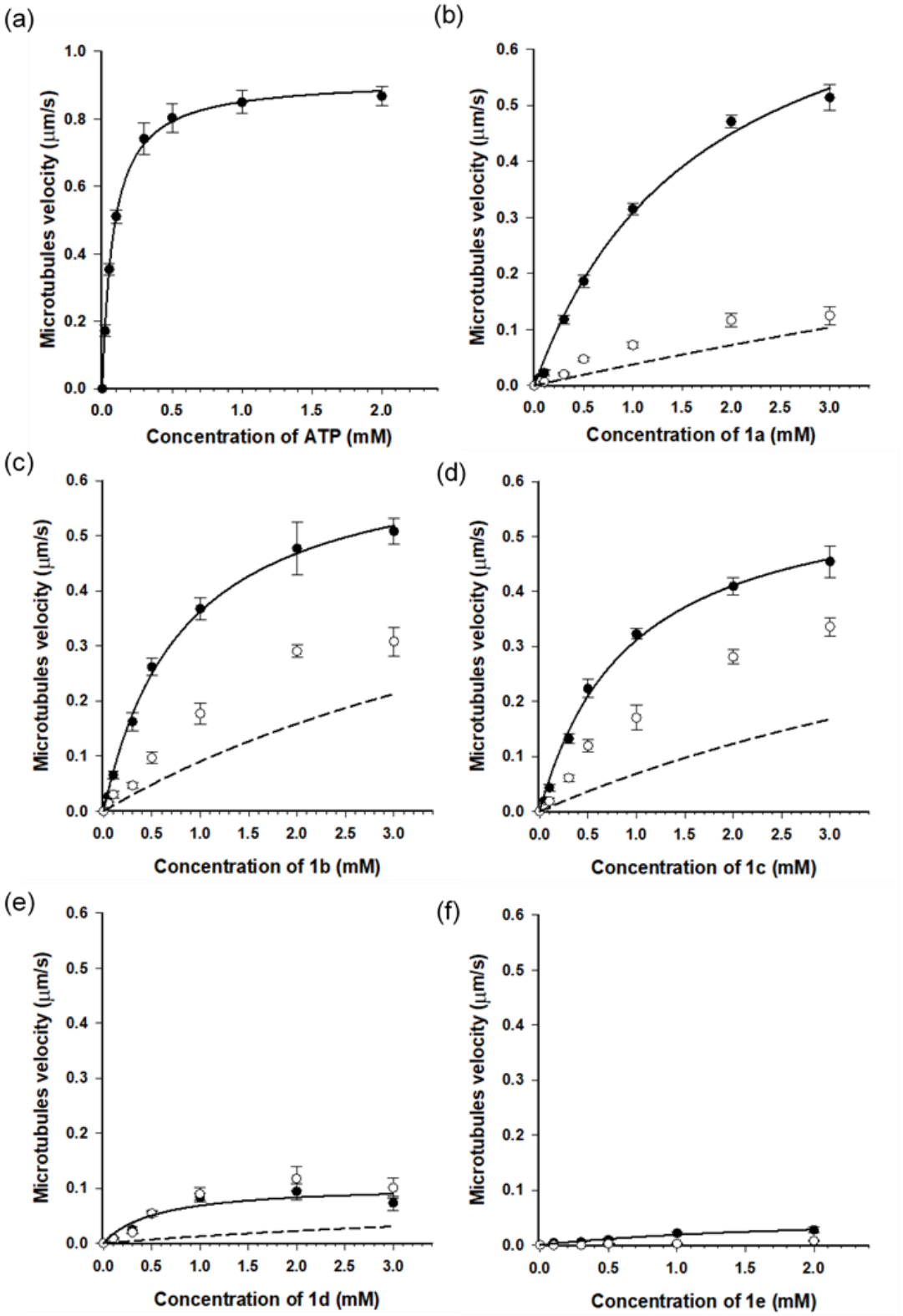

Fig. 2.6 Microtubules gliding velocity (filled circle (●): BI condition and open circle (○): UV condition) with AzoTP derivatives (a) ATP, (b) **1a**, (c) **1b**, (d) **1c**, (e) **1d**

and (f) **1e**[15]. Solid black line: curve fitting using the Michaelis-Menten equation (K_m = 0.079 ± 0.003 mM, V_{max} = 0.92 ± 0.01 µm/sec for ATP, K_m = 1.7 ± 0.2 mM, V_{max} = 0.83 ± 0.06 µm/sec for **1a**, K_m = 0.82 ± 0.07 mM, V_{max} = 0.66 ± 0.02 µm/sec for **1b**; K_m = 0.93 ± 0.09 mM, V_{max} = 0.60 ± 0.02 µm/sec for **1c**, and K_m = 1.0 ± 0.4 mM, V_{max} = 0.15 ± 0.03 µm/sec for **1d**; K_m = 2.1 ± 1 mM, V_{max} = 0.058 ± 0.02 µm/sec for **1e**). Dash black line: theoretical curve calculated from the remaining *trans* isomer in *cis* rich state of the respective AzoTP derivatives. Error bars represent the standard deviation of 10 microtubules in a single flow cell.

Photoswitchability of gliding velocity of microtubules by alternating illumination with UV and VIS light was also studied. AzoTP derivatives **1b** (0.51 µm/sec at 3.0 mM) and **1c** (0.45 µm/sec at 3.0 mM) exhibited comparable velocity with **1a** at BI condition. Upon the subsequent UV irradiation, the gliding velocity decreased to 0.31 µm/sec at 3.0 mM with **1b** and 0.34 µm/sec at 3.0 mM with **1c** (Fig. 2.6 b, c and d), but their changes between BI and UV condition were not drastic compared with actin-myosin system (Table 2.2 and Fig. 2.5). The reversible photoswitching of microtubules gliding velocity using **1b** and **1c** was also achieved with alternating irradiation of UV and VIS light (Fig. 2.7,). These results indicated that the flexibility and length of linker chains between the azobenzene moiety and triphosphate group (acetamide linker for **1a**, ethyl linker for **1b** and propyl linker for **1c**) have the trivial effect on powering the microtubule-kinesin system. AzoTP **1d** with the ethyl ether linker showed less activity (BI : 0.07 µm/sec at 3.0 mM) than the original AzoTP **1a**. There was no significant change in the microtubules velocity between BI and UV condition (UV : 0.10 µm/sec at 3.0 mM) although the clear photo isomerization from *trans* isomer to *cis* isomer was confirmed by the UV-VIS spectra (Fig. 2.2c,).

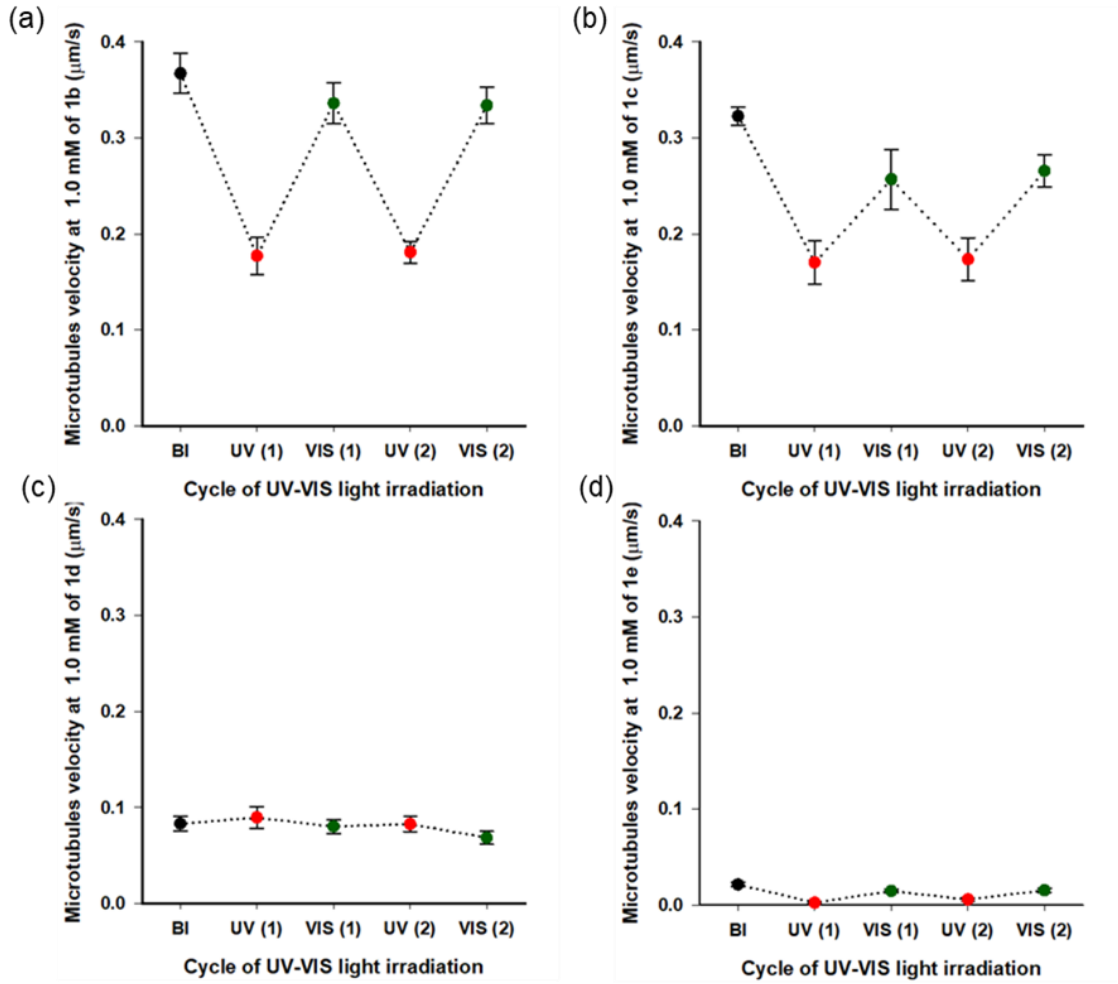

Fig. 2.7 Reversible photoregulation of the microtubule gliding velocity induced by AzoTP derivatives. (BI: before irradiation; UV: after irradiation with 365 nm light; Vis: after irradiation with 436 nm light). (a) **1b**, (b) **1c**, (c) **1d** and (d) **1e**. Error bars represent the standard deviation of 10 microtubules in a single flow cell.

The ethyl ether linker in **1d** was almost same length with the propyl linker in **1c**, but it was found that the oxygen atom in the ether group of **1d** negatively affected the powering activity and photoswitchability in microtubule-kinesin system. This might be because the ether group worked as the acceptor of hydrogen bonding, which could interrupt the substrate recognition of **1d** by kinesin. To quantitatively assess the powering ability of *cis*-isomers of AzoTPs in

microtubule-kinesin system, the author plotted theoretical curves (dash black line in Fig. 2.6b-e) corresponding to the remaining *trans* isomer (Table 2.1) of AzoTPs at UV irradiation condition. Inconsistency in **1b**, **1c** and **1d** between the theoretical curves and the actual velocity under UV condition implied that the *cis* isomers had significant activity on gliding motility. In contrast with **1a**-**1d** (0.47 μm/sec for **1a**, 0.48 μm/sec for **1b**, 0.41 μm/sec for **1c** and 0.09 μm/sec for **1d** at 2.0 mM concentration), to our surprise, **1e** with two methyl groups in azobenzene moiety showed almost no powering activity (0.027 μm/sec at 2.0 mM) and photoswitchability towards kinesin-1 (Fig. 2.6f and Fig. 2.8)[15]. Representative fluorescence images of the gliding motility of microtubules with **1e** at 8 min interval for both in the BI state and after UV illumination state were shown in Fig. 2.8. V_{max} (0.058 μm/sec) with **1e** was only 6.3 % of V_{max} (0.92 μm/sec) with ATP (Fig. 2.6a) in the microtubule-kinesin motility assay. Therefore, the author concluded that the methyl substitution critically impeded the substrate recognition of AzoTP in the kinesin motor.

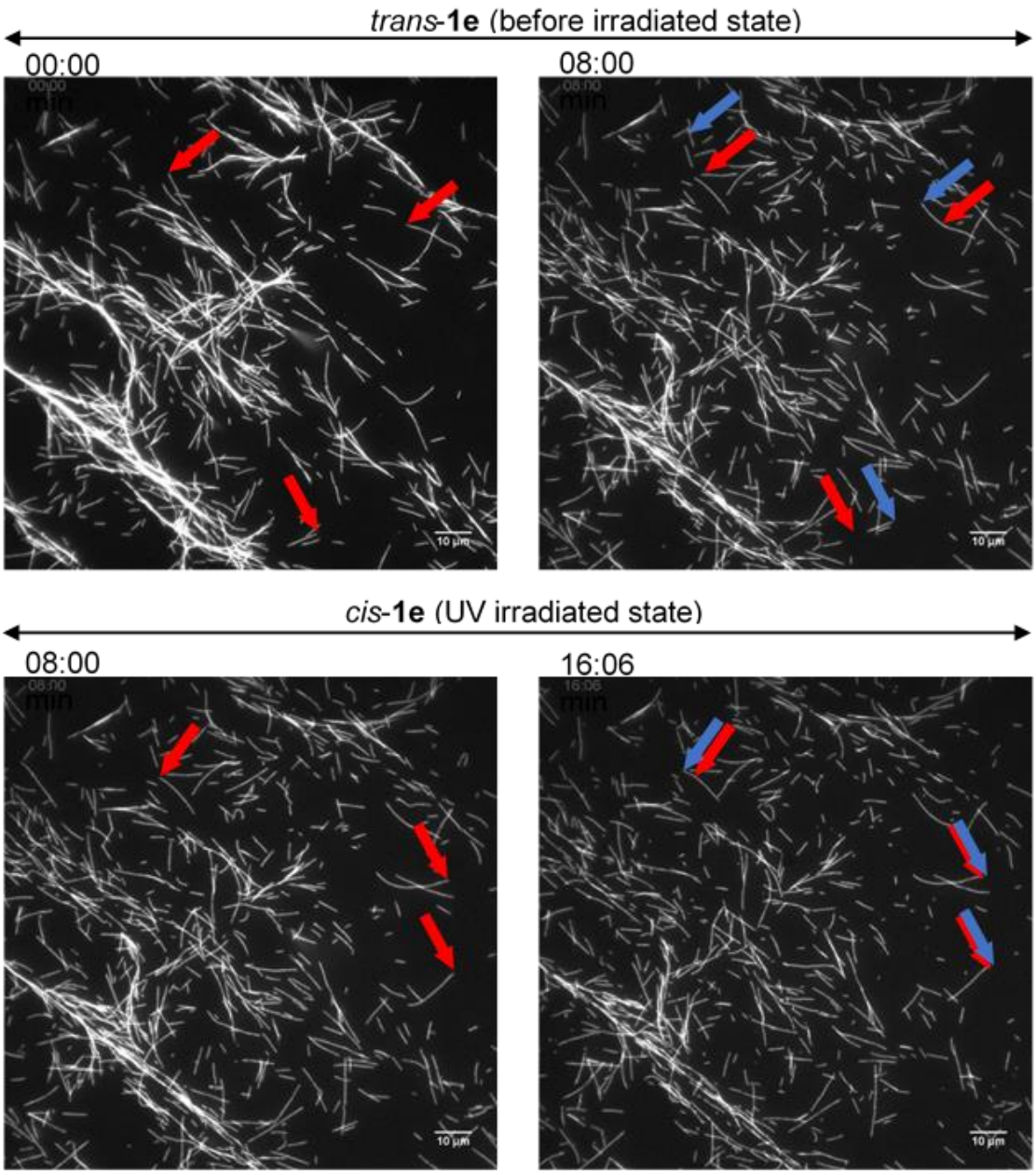

Fig. 2.8 Fluorescence images of the gliding microtubules driven by **1e** (2.0 mM) on microtubule-kinesin gliding motility assay. (Top) Before irradiated state; (bottom) after UV irradiated state; (left side) starting frame; (right side) frame after 8 min; Red arrows: leading points of the microtubules at starting frame; blue arrows: leading points of the same microtubules after 8 min.

2.2.4. Comparison of AzoTP molecules between myosin and kinesin system

Guanosine triphosphate (GTP) has been reported as a kinesin-selective natural nucleoside triphosphate (NTP)[5,9]. The author also confirmed the kinesin selectivity of GTP in our motility system.

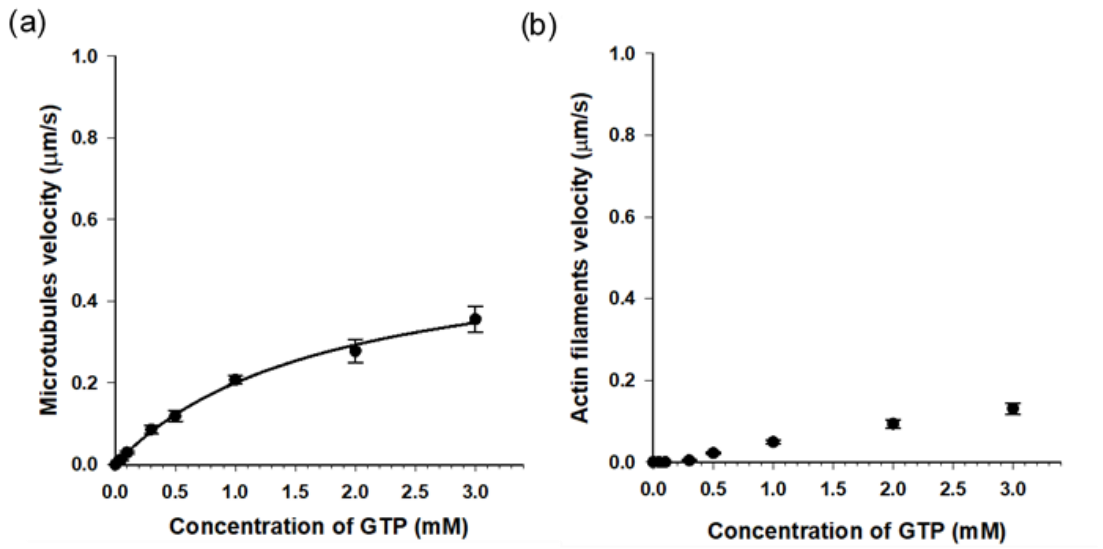

Fig. 2.9 Microtubule or actin filament gliding motility with GTP. (a) Gliding velocity of microtubules depending on the concentration of GTP in microtubule-kinesin system. Solid black line: curve fitting using the Michaelis-Menten equation (K_m = 1.8 ± 0.2 mM, V_{max} = 0.55 ± 0.03 μm/sec) (b) Gliding velocity of actin filaments with respect to the concentration of GTP in actin-myosin system. Error bars represent the standard deviation of 10 actin filaments in a single flow cell.

GTP could power kinesin to drive microtubules efficiently (0.21 μm/sec at 1.0 mM), whereas it could not work efficiently (0.049 μm/sec at 1.0 mM) in actin-myosin motility system (Fig. 2.9). This special trend encouraged us to compare AzoTPs in both of myosin and kinesin systems in a quantitative way.

To directly demonstrate the powering activities and efficiencies of our AzoTPs for myosin and kinesin, ATP was used as the standard substrate for both the kinesin and myosin motor protein system (Table 2.4).

Table 2.4 Summary of efficacy of AzoTP molecules as photo-responsive energy molecule in microtubule-kinesin and actin-myosin system

NTPs/ AzoTPs	Microtubule-kinesin system		Actin-myosin system		Activity specificity (Myo/Kin) under BI condition
	MTs velocity [a] (μm/sec)		F-actin velocity [b] (μm/sec)		
	BI	UV*	BI	UV*	
ATP	0.92 ± 0.01 (100%)	0.92 ± 0.01 (100%)	2.9 ± 0.1[2] (100%)	2.9 ± 0.1[2] (100%)	1.0
GTP	0.55 ± 0.03 (60%)	0.55 ± 0.03 (60%)	0.049 ± 0.01[c] (1.0%)	0.049 ± 0.01[c] (1.0%)	0.02
1a	0.83 ± 0.06 (90%)	0.12 ± 0.01 (13%)	1.5 ± 0.04[2] (52%)	0.84 ± 0.1[2] (29%)	0.6
1b	0.66 ± 0.02 (72%)	0.31 ± 0.03 (34%)	1.0 ± 0.1[2] (35%)	0.13 ± 0.02[2] (4.5%)	0.5
1c	0.60 ± 0.02 (65%)	0.34 ± 0.02 (37%)	1.4 ± 0.2 [d] (27%)	0.34 ± 0.03 [d] (6.7%)	0.4
1d	0.15 ± 0.03 (16%)	0.10 ± 0.02 (11%)	1.9 ± 0.1[2] (66%)	0.38 ± 0.04[2] (13%)	4.1
1e	0.058 ± 0.02 (6.3%)	N.D.	1.7 ± 0.2[2] (59%)	0.39 ± 0.05[2] (13%)	9.4

[a] Microtubules (MTs) velocity at V_{max}. [b] F-actin filaments (F-actin) velocity at V_{max}.

* Under UV condition, the saturated concentration of AzoTPs in the corresponding motility assays was considered. [c] Velocity at 1.0 mM of GTP was considered because V_{max} is not determinable due to too low activity. [d] The different V_{max} (5.1 ± 0.2 μm/sec) of ATP was used for the calculation, because The author used the different batch of myosin and actin from our previous report in this new experiments. Activity specificity, Myo/Kin is ratio of myosin driven actin filaments standardized velocity and kinesin driven microtubules

standardized velocity at V_{max}. The standardized velocity is shown in the parentheses with the actual velocity where the V_{max} of ATP is considered as standard velocity (100%) for each of the motor protein system. N.D. : Not Determined.

AzoTPs (**1a**-**1d**) exhibited the moderate activity towards both of myosin (> 27% V_{max} of ATP) and kinesin (> 16% V_{max} of ATP). However, AzoTP **1e** showed the different trends toward myosin and kinesin. In the myosin, **1e** showed 59% of V_{max} and 16% of $1/K_m$ (3.7 mM^{-1}) compared with ATP. In the kinesin, **1e** showed 6.3% of V_{max} and 3.8% of $1/K_m$ (0.48 mM^{-1}) compared with ATP. This high activity specificity of **1e** (Myo/Kin = 9.4) with high photoswitchability (Table 2) indicated that **1e** was recognized as a substrate of not kinesin-1 but myosin II, although other AzoTPs (**1a**-**1d**) worked as substrates for both motor proteins.

2.2.5. Computational docking simulation of AzoTP derivatives with the motor domain of kinesin-1 and myosin II

Since **1e** displayed the high selectivity towards myosin II compared with kinesin-1, the putative binding modes of AzoTPs **1a** (the good substrate for both kinesin and myosin) and **1e** with kinesin-1 and myosin II were investigated through the docking simulations (Fig. 2.10-2.12).

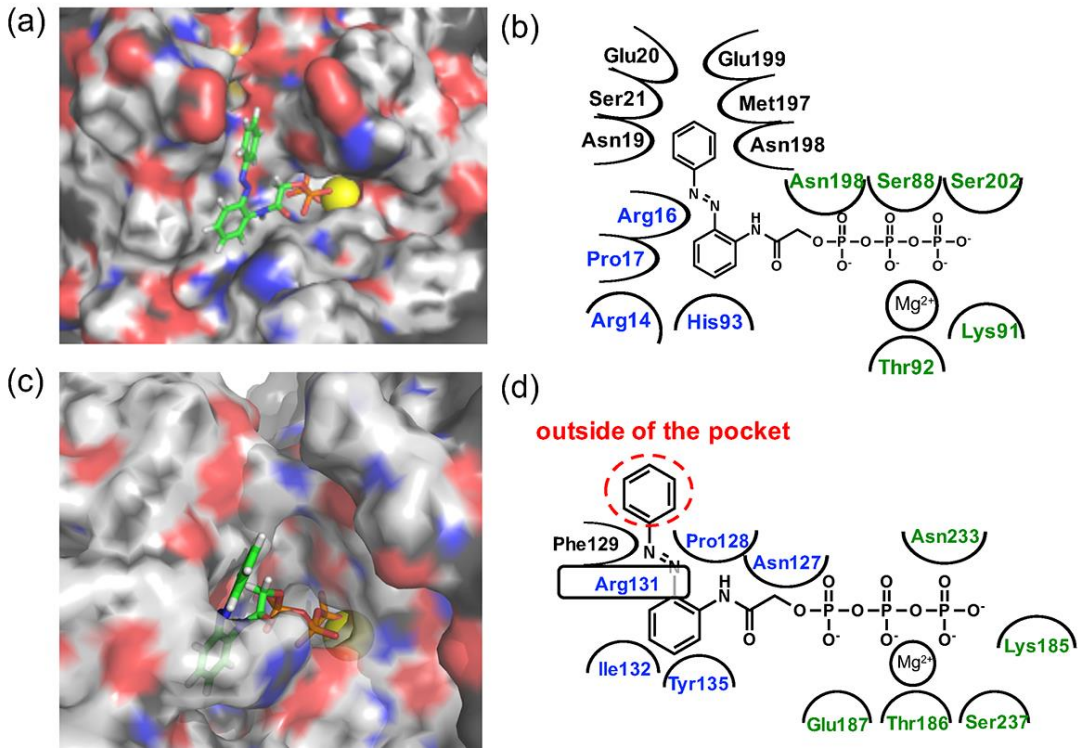

Fig. 2.10 Computational docking simulation of *trans* isomers of **1a** with kinesin-1 and myosin II motor domain. Docking simulation of AzoTPs was conducted with CLC Drug Discovery Workbench (QIAGEN). X-ray crystal structures obtained from RCSB Protein Data Bank (PDB entry code: 4HNA for kinesin-1 and 1MMD for myosin II) were used. All figures of simulated results were created with pymol (DeLano Scientific). (a) Simulated result and (b) binding modes of *trans* isomer of **1a** in kinesin-1. (c) Simulated result and (d) binding modes of *trans* isomer of **1a** in myosin II. In simulated results, AzoTPs were represented by a stick mode. Magnesium ion was done by a yellow ball. In the figures of binding modes, the amino acid resides composing ARBS were colored in blue and the residues composing the triphosphate binding site were colored in green.

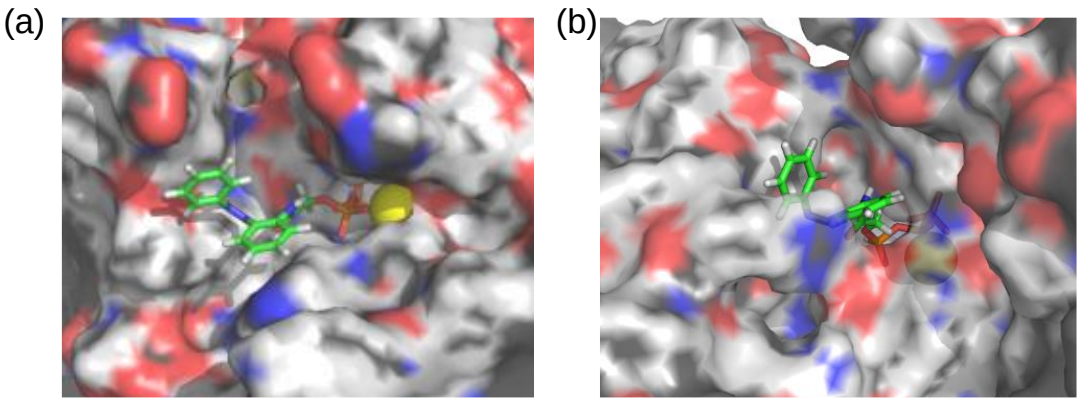

Fig. 2.11 Computational docking simulation of *cis* isomers of **1a** with (a) kinesin-1 and (b) myosin II motor domains.

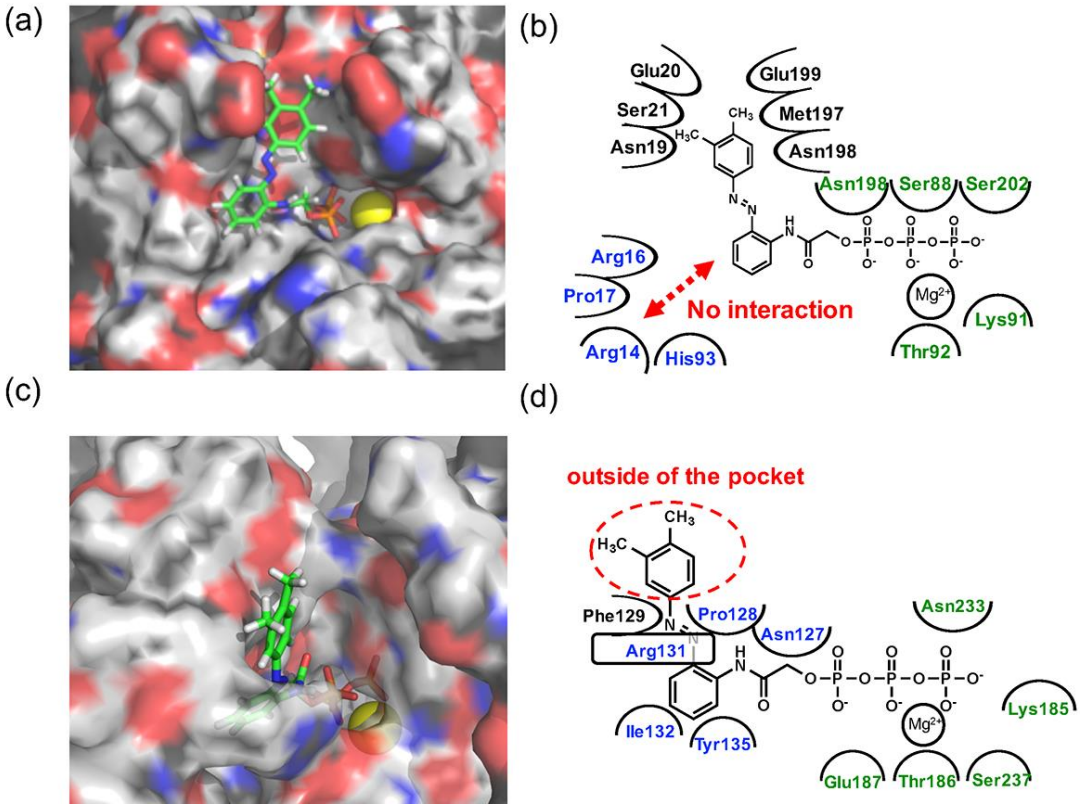

Fig. 2.12 Computational docking simulation of *trans* isomers of **1e** with kinesin-1 and myosin II motor domain. Docking simulation of AzoTPs was conducted with CLC Drug Discovery Workbench (QIAGEN). X-ray crystal structures obtained from RCSB Protein Data Bank (PDB entry code: 4HNA for kinesin-1 and 1MMD for myosin II) were used. All figures of simulated results were created

with pymol (DeLano Scientific). (a) Simulated result and (b) binding modes of *trans* isomer of **1e** in kinesin-1. (c) Simulated result and (d) binding modes of *trans* isomer of **1e** in myosin II. In simulated results, AzoTPs were represented by a stick mode. Magnesium ion was done by a yellow ball. In the figures of binding modes, the amino acid resides composing ARBS were colored in blue and the residues composing the triphosphate binding site were colored in green.

In the simulation results of kinesin-1 and myosin II with *trans* isomer of **1a**, triphosphate groups were chelated with magnesium ion at the same binding site of triphosphate group in ATP (Fig. 2.10a and b). In the azobenzene moiety, the benzene ring connected with triphosphate group through an acetamide linker was well-overlapped with the adenine ring of ADP in the original X-ray structures of both of kinesin and myosin (Fig. 2.13).

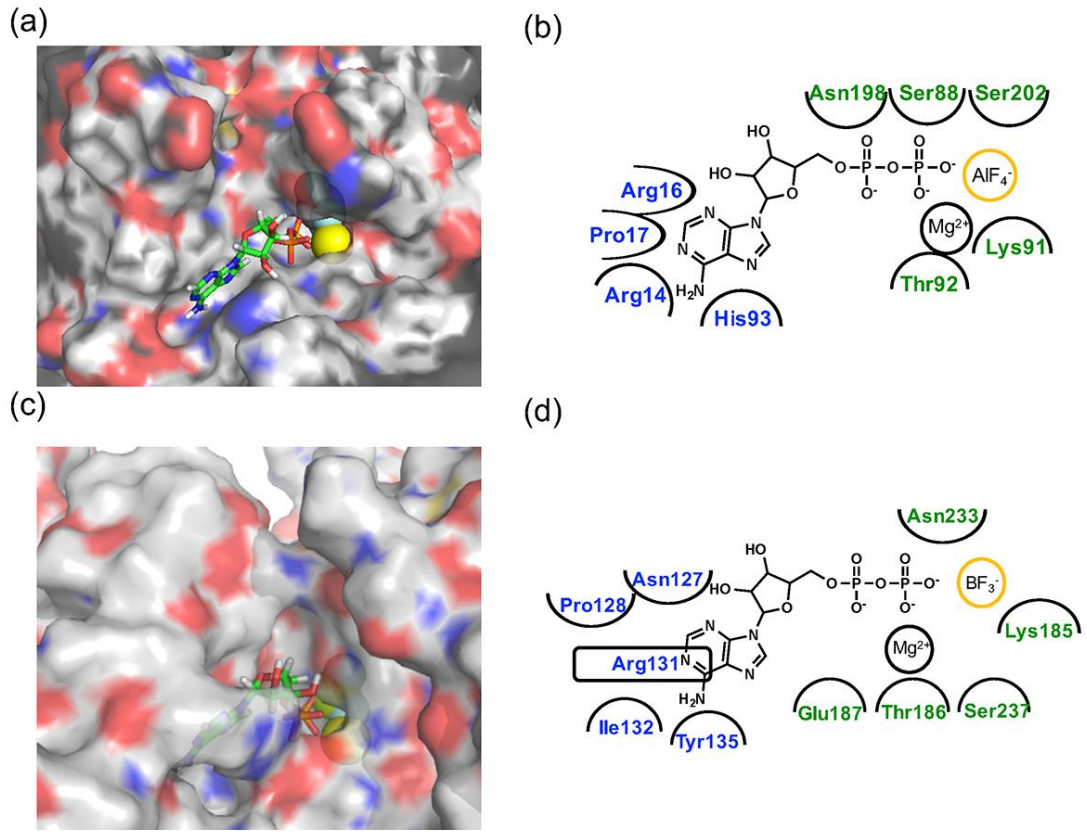

Fig. 2.13 X-ray crystallography analyses of ATP analogues with kinesin-1 and myosin II motor domain. X-ray crystal structures obtained from RCSB Protein Data Bank (PDB entry code: 4HNA for kinesin-1 and 1MMD for myosin II) were used. All figures of simulated results were created with pymol (DeLano Scientific). (a) X-ray structure and (b) binding modes of ADP-Mg-AlFx in kinesin-1. (c) X-ray structure and (d) binding modes of ADP-Mg-BFx in myosin II. In X-ray structures, ADP were represented by a stick mode. Magnesium ion (yellow) and BF_3^- or AlF_4^- was done by a ball mode. In the figures of binding modes, the amino acid resides composing ARBS were colored in blue and the residues composing the triphosphate binding site were colored in green.

In myosin, azo group (-N=N-) can interact via a hydrogen bond with Arg131 of covering the adenine ring binding site (ARBS), which could fix the angle of the azobenzene moiety. Another benzene ring in the azobenzene moiety was located outside of the ATP binding site to face the solvent direction. Therefore, it was likely that there was no interaction of that benzene ring with the surrounding amino acids. In kinesin, His93 was the key residue for exhibiting ATPase activity[3]. From the simulation, the benzene unit in **1a** was estimated to show the π-π interaction with His93 as well as ATP. Due to no amino acids covering ARBS unlike myosin, the azo group (-N=N-) was relatively flexible. This flexibility possibly contributed to arranging the outside benzene ring of the azobenzene moiety not to facing the solvent direction but to being buried in other space near the ATP binding site (Figure 2.10b). Despite of slightly different binding modes of *trans* isomer of **1a** with kinesin and myosin, these well-fittings were robustly consistent with the results on the motility assays that **1a** exhibited the relatively high activities for powering kinesin (4.7% of $1/K_m$ and 90% of V_{max}

compared with ATP) and myosin (43% of $1/K_m$ and 52% of V_{max} compared with ATP) under BI condition. Conversely, *cis* isomer of **1a** has almost no contribution to the gliding velocity of cytoskeletal filaments in both of the motor protein systems[1,2]. We also docked the *cis* isomer of **1a** with kinesin and myosin for explaining the low affinity of *cis* isomer of **1a** in kinesin and myosin. As shown in Fig. 2.11a and b, the total incompatibility of *cis* isomer of **1a** in ARBS was observed, although the triphosphate group was well-bound. This suggested that the bent azobenzene unit prevented the approaches of **1a** into ARBS. Almost similar binding modes of AzoTPs were applied except for **1e**, which exhibited the high selectivity to myosin over kinesin. In the docking results of *trans* isomer of **1e** with myosin, the benzene ring in **1e** was well-occupied with ARBS as well as other AzoTPs and the dimethyl-substituted benzene ring was located facing to solvents (Fig. 2.12). In contrast, the docking of **1e** with kinesin showed the incompatibility of the benzene ring of the azobenzene moiety with ARBS, because the steric hindrance of two methyl groups on the azobenzene moiety interrupted the access of **1e** to ARBS. Thus, these computational docking studies could explain our experimental results of myosin selectivity in **1e** over kinesin.

2.2.6. Selective photoregulation of myosin motility using 1e in kinesin-myosin composite motility assay

Since **1e** exhibited the high selectivity to myosin over kinesin, the selective photoregulation of myosin was explored in kinesin-myosin composite motility assay[4], where both kinesin and myosin were attached on the same glass surface and microtubules and actin filaments were glided over the motor proteins. The gliding motility of fluorescence labeled microtubules and actin filaments driven by respective motor proteins was observed with the fluorescence microscope.

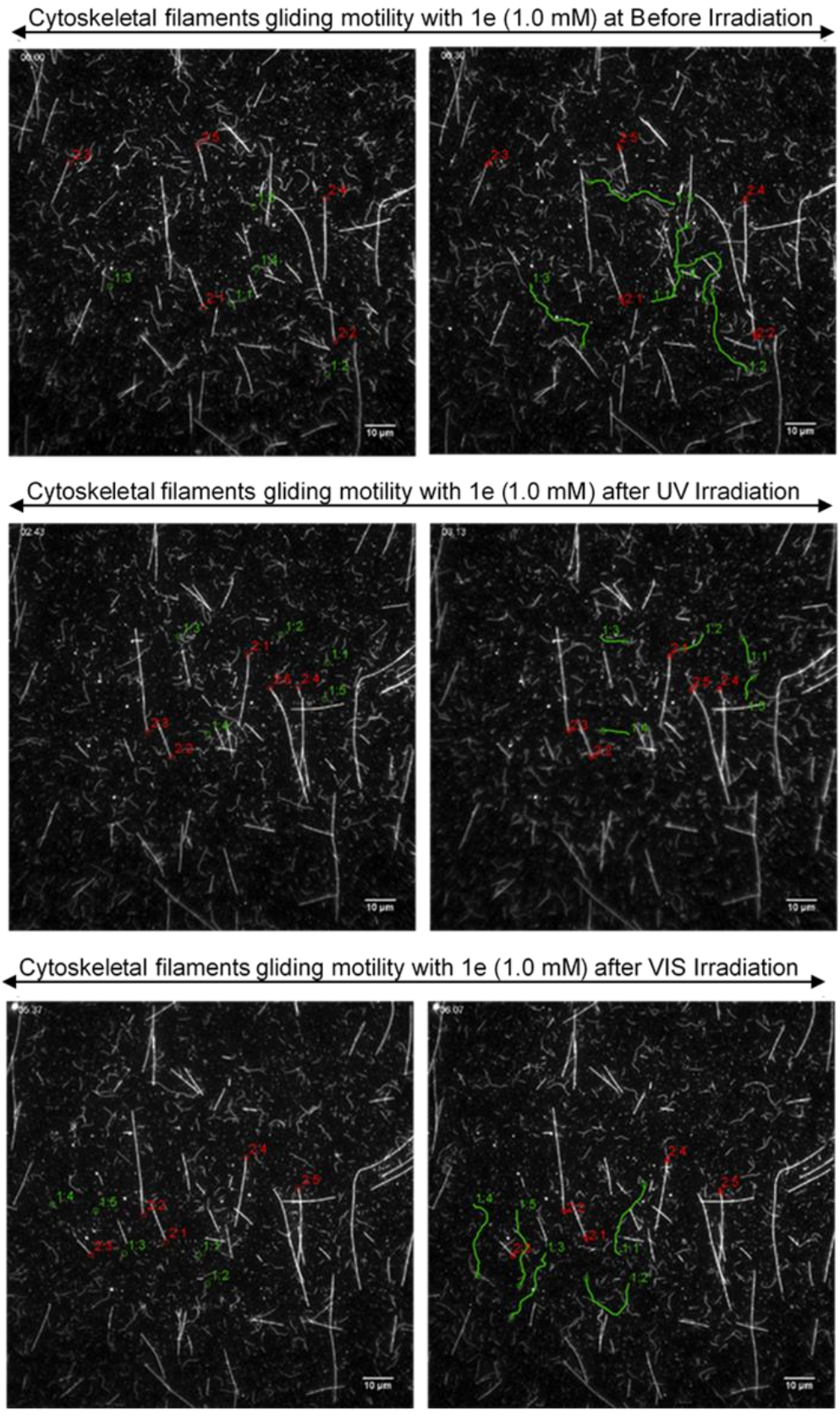

Fig. 2.14 Fluorescence images of the gliding actin filaments and microtubules driven by **1e** (1.0 mM) on kinesin-myosin composite motility assay. (Top) Before

irradiation, *trans* state; (middle) *cis*-rich state after UV irradiation; (bottom) *trans*-rich state after VIS light irradiation; (left side) starting frame; (right side) frame after 30 sec. The distance traveled by five actin filaments (green lines) and five microtubules (red lines) were shown using tracking the path of each actin filament or microtubule tails.

The gliding motility of microtubules and actin filaments in the kinesin-myosin composite assay with **1e** (1.0 mM) was examined under different light irradiation conditions (Fig. 2.14). AzoTP **1e** could power myosin to drive actin filaments with photoreversibility (BI : 1.1 ± 0.04 μm/sec, UV : 0.27 ± 0.01 μm/sec and VIS : 0.88 ± 0.03 μm/sec at 1.0 mM) in the composite motility assay. In contrast, it could not power kinesin efficiently to drive microtubules (BI : 0.054 ± 0.01 μm/sec at 1.0 mM). As the control experiment, ATP (0.2 mM) was applied to our kinesin-myosin composite system. It was shown that both kinesin and myosin motors were driven efficiently to afford the velocity of microtubules (0.71 ± 0.02 μm/sec) and actin filaments (3.3 ± 0.3 μm/sec). These findings suggested that AzoTP **1e** also worked as the photoswitchable substrate with myosin specificity in kinesin-myosin composite motility assay.

2.3. Conclusion

The myosin-specific AzoTP molecule **1e** with high photoswitchability was discovered through studying the powering activity of several AzoTPs in the kinesin and myosin motility assays, respectively. Even in the kinesin-myosin composite system, **1e** could drive the myosin selectively. This myosin selectivity in **1e** was explained by its binding modes with kinesin or myosin motors through the docking simulation. This rational analysis of binding modes of AzoTPs using both of the experimental assays and the computational studies might contribute to the other motor-specific substrate molecules.

2.4. Materials and methods

2.4.1. Chemicals

All chemical and biochemical reagents were purchased from commercial sources (Wako Pure Chemical, Kanto Chemical, TCI Chemical, Sigma-Aldrich, Biotium and Dojindo Molecular Technologies) and used without further purification. Thin-layer chromatography (TLC) was performed on silica gel 60 F_{254}-precoated aluminum sheets (Merck) and visualized by fluorescence. Chromatographic purification was performed using flash column chromatography on silica gel 60 N (neutral, 63−210 μm, Kanto Chemical).

2.4.2. General methods, instrumentation and measurements

NMR spectroscopy (^{1}H, ^{13}C and ^{31}P) was performed on a 400 MHz spectrometer (ECX-400, JEOL). ^{1}H NMR measurements were carried out using $CDCl_3$, CD_3OD and D_2O as solvent and tetramethylsilane (TMS) as an internal standard. For ^{13}C and ^{31}P NMR, D_2O was used as solvent while methanol as an internal standard for ^{13}C and phosphoric as an external standard for ^{31}P NMR. Chemical shift data are given in units of parts per million (ppm) relative to the standard. Purity of AzoTP molecules was analyzed using a reversed phase HPLC system (Prominence, Shimadzu). High-resolution mass spectroscopy (HR-MS) experiments were performed by using Thermo Scientific Exactive mass spectrometer with electrospary ionization. A FDU-2200 (EYELA) lyophilization system was used for freeze-drying. UV-Visible spectrophotometry was carried out on a UV-1800 (Shimadzu) UV-Visible spectrophotometer, in stoppered 1 mm path length quartz cells. *cis-trans* photoisomerization of AzoTP derivatives was performed by using a 365 nm UV LED (C11924-101, Hamamatsu) and a mercury

lamp (Ushio) with proper bandpass filter for 436 nm. Fluorescent imaging of *in vitro* gliding motility assay (kinesin-microtubule, myosin-actin and kinesin-myosin composite) was performed in an EMCCD digital camera (DL-604M-0EM-H1, Andor Technology) equipped epifluorescence microscope (IX71, Olympus) with a 60×/1.45 NA oil-immersion objective lens (PlanApo, Olympus) and appropriate excitation filter set for 640 nm light from a mercury lamp.

2.4.3. Synthesis of AzoTP molecules

The general synthetic route for AzoTP molecules involves multi-step synthesis. The AzoTP molecules, **1a**, **1b**, **1d** and **1e** were synthesized as described in our previous report[1,2]. The new AzoTP, **1c** was synthesized as depicted in Scheme 2.1 with details of synthetic procedure.

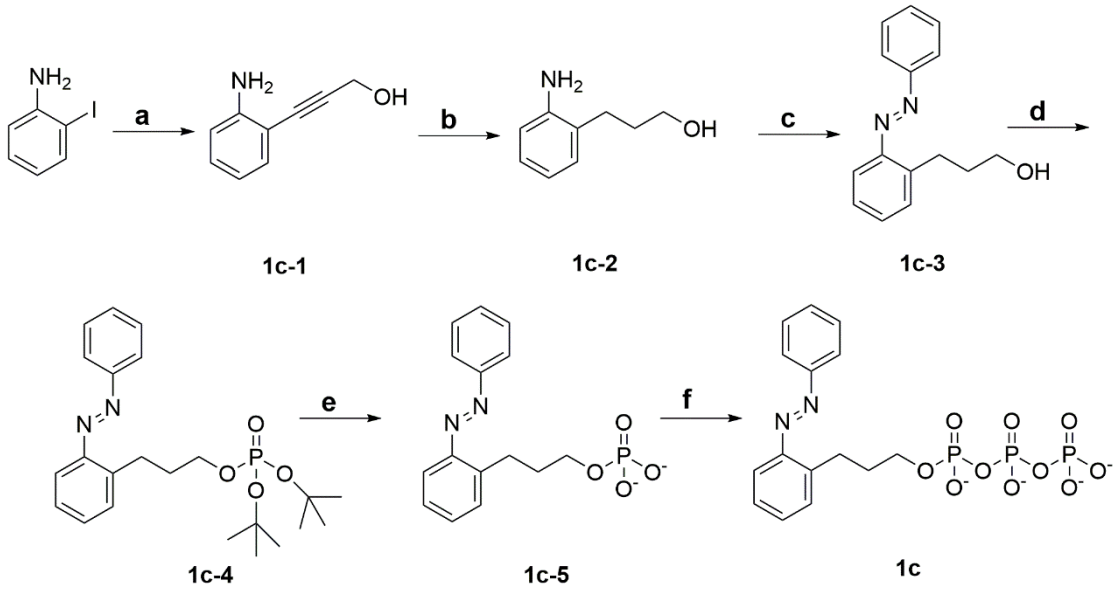

Scheme 2.1 Synthetic scheme of 1c. Reagent and condition: (a) CuI, bis(triphenylphosphine)palladium(II) dichloride, 2-propyn-1-ol, triethylamine,

RT,18 h. (b) 10% Pd/C, H_2, MeOH, RT, 48 h. (c) Nitrosobenzene, AcOH, toluene, N_2 atmosphere, 60 °C, 21 h. (d) Di-tert-butyl N,N-diisopropylphosphoramidite,1H-tetrazol, dry THF, Ar atmosphere, RT, 6 h, then mCPBA, 0 °C, 1 h. (e) TFA, dry DCM, Ar atmosphere, RT, 6 h. (f) Tributylamine, carbonyldiimidazole, tributylammonium pyrophosphate, dry DMF, Ar atmosphere, RT, overnight.

3-(2-aminophenyl)prop-2-yn-1-ol (**1c-1**)**:**

A reaction mixture of copper (I) iodide (32 mg, 0.2 mmol), bis(triphenylphosphine)palladium(II) dichloride (140 mg, 0.2 mmol), and 2-iodoaniline (4.4 g, 20 mmol) in 120 mL of triethylamine were stirred under Ar atmosphere. After 30 min of stirring, 2-propyn-1-ol (1.2 mL, 20 mmol) was added to the reaction mixture and it was kept stirring for 18 h at room temperature. The reaction mixture was evaporated and partitioned between water and DCM. The DCM part was washed several times with water to remove triethylamine completely then dried over $MgSO_4$ and concentrated. The residue was purified by silica gel column chromatography (MeOH/DCM, 3/97) to afford 1.95 g (65 %) of a maroon solid 3-(2-aminophenyl)prop-2-yn-1-ol (**1c-1**). ^{1}H NMR (400 MHz, CHLOROFORM-D) δ 7.28 (d, *J* = 1.3 Hz, 1H), 7.13 (t, *J* = 7.9 Hz, 1H), 6.70 – 6.66 (m, 2H), 4.55 (d, *J* = 4.0 Hz, 2H), 4.21 (br, 2H), 1.70 (br, 1H).

3-(2-aminophenyl)propan-1-ol (1c-2):

A solution of **1c-1** (1.95 g, 13.2 mmol) in dry MeOH (60 mL) was added to 10 % Pd/C (0.5 g) under N_2 atmosphere at room temperature. Then N_2 gas was changed to H_2 gas with a constant pressure from a rubber bladder. The reaction mixture was stirred for 48 h and filtered through celite pad. The solvent was

evaporated and the residue was purified by silica gel column chromatography (hexane/EtOAc, 1/1) to afford 1.03 g (51 %) of 3-(2-aminophenyl)propan-1-ol (**1c-2**) as a dark brown solid**.** ^{1}H NMR (400 MHz, CHLOROFORM-D) δ 7.06 – 7.02 (m, 2H), 6.76 (td, *J* = 7.4, 1.2 Hz, 1H), 6.69 (d, *J* = 7.4 Hz, 1H), 3.64 (t, *J* = 6.0 Hz, 2H), 2.64 (t, *J* = 7.3 Hz, 2H), 1.87 (quin, *J* = 6.5 Hz, 2H), 1.67 (br, 1H).

(E)-3-(2-(phenyldiazenyl)phenyl)propan-1-ol (1c-3):

A solution of **1c-2** (0.276 g, 1.8 mmol) in toluene (13 mL) was degassed under a stream of N_2 gas for 15 min. To the solution, nirtosobenzene (0.193 g, 1.8 mmol) and acetic acid (0.5 mL) were added under Ar atmosphere. The reaction mixture was stirred at 60 °C for 21 h. The solvent of the reaction mixture was evaporated and partitioned between water and DCM. The DCM part was washed several times with water and dried over $MgSO_4$. The solvent was evaporated *in vacuo*. The residue was purified by silica gel column chromatography (hexane/EtOAc, 4/3) to afford 0.374 g (86 %) of (*E*)-3-(2-(phenyldiazenyl)phenyl)propan-1-ol (**1c-3**) as a dark brown solid. ^{1}H NMR (400 MHz, CHLOROFORM-D) δ 7.89 (dd, *J* = 8.3, 1.4 Hz, 2H), 7.67 (dd, *J* = 8.0, 1.2 Hz, 1H), 7.56 – 7.46 (m, 3H), 7.44 – 7.36 (m, 2H), 7.31 (t, *J* = 7.5 Hz, 1H), 3.63 (q, *J* = 6.1 Hz, 2H), 3.24 (t, *J* = 7.2 Hz, 2H), 2.05 (t, *J* = 6.1 Hz, 1H), 1.97 (quin, *J* = 6.6 Hz, 2H).

(*E*)-di-*tert*-butyl (3-(2-(phenyldiazenyl)phenyl)propyl) phosphate (1c-4):

To a solution of **1c-3** (1.22 g, 5.1 mmol) and di-*tert*-butyl *N*,*N*-diisopropylphosphoramidite (2.1 mL, 6.5 mmol) in dry THF (20 mL), 1*H*-tetrazole (1.04 g, 15.0 mmol) was added. The reaction mixture was stirred for 7 h at room temperature. A solution of *m*-chloroperoxybenzoic acid (65%, 2.3 g, 8.6 mmol) in dry CH_2Cl_2 (10 mL) was added. The mixture was stirred for 1 h in an ice bath

and then for 30 min at room temperature. Saturated aqueous $NaHCO_3$ (60 mL) was added and the mixture was stirred for further 30 min. The reaction mixture was partitioned between EtOAc and water. The organic phase was washed with brine (once), dried over $MgSO_4$ and concentrated. The residue was purified through silica gel column chromatography (hexane/EtOAc, 3/2) to afford 1.18 g (38 %) of (*E*)-di-*tert*-butyl (3-(2-(phenyldiazenyl)phenyl)propyl) phosphate (**1c-4**) as a red oil. ^{1}H NMR (400 MHz, CHLOROFORM-D) δ 7.92 (dd, *J* = 8.3, 1.4 Hz, 2H), 7.67 (d, *J* = 7.8 Hz, 1H), 7.55 – 7.34 (m, 5H), 7.33 – 7.28 (m, 1H), 4.03 (q, *J* = 6.4 Hz, 2H), 3.25 (t, *J* = 7.7 Hz, 2H), 2.06 (quin, *J* = 7.2 Hz, 2H), 1.47 (s, 18H).

(*E*)-3-(2-(phenyldiazenyl)phenyl)propyl phosphate (1c-5):

Trifluoroacetic acid (1.8 mL) was added to a solution of compound **1c-4** (0.65 g, 1.5 mmol) in dry DCM (16 mL). The reaction mixture was stirred for 6 h at room temperature. MeOH (30 mL) was added and the mixture was evaporated. This procedure was repeated several times to remove CF_3COOH completely. The residue was dried *in vacuo*. Water (5 mL) was added to the residue and neutralized with 1 M NaOH. This crude product was purified by DEAE Sephadex A-25 column with 0.5 M triethylammonium hydrogencarbonate (TEAB) buffer (pH 8.0) as an eluent at 4 °C. The fractions containing the product were coevaporated with EtOH to remove water and TEAB to afford 0.60 g (96 %) of (*E*)-3-(2-(phenyldiazenyl)phenyl)propyl phosphate (**1c-5**) (triethyl ammonium salt) as a red oil. ^{1}H NMR (400 MHz, CD_3OD) δ 7.91 (dd, *J* = 8.4, 1.3 Hz, 2H), 7.65 (d, *J* = 7.9 Hz, 1H), 7.57 – 7.41 (m, 5H), 7.29 (t, *J* = 8.4 Hz, 1H), 3.94 (q, *J* = 6.4 Hz, 2H), 3.26 (t, *J* = 7.8 Hz, 2H), 3.17 (q, *J* = 7.3 Hz, 6H), 2.00 (quin, *J* = 7.1 Hz, 2H), 1.29 (t, *J* = 7.3 Hz, 9H).

(*E*)-3-(2-(phenyldiazenyl)phenyl)propyl triphosphate, AzopropylTP (1c):

The triethylammonium salt of compound **1c-5** (0.58 g, 1.4 mmol) was converted into its tributylammonium salt through the addition of tributylamine (1 mL, 4 mmol) in dry MeOH (7 mL). Triethylamine and MeOH were evaporated. The tributylammonium salt was dissolved in dry DMF (12 mL). While stirring, a solution of 1,1´-carbonyldiimidazole (1.2 g, 7.5 mmol) in dry DMF (10 mL) was added under Ar atmosphere and then the reaction was left for 16 h at room temperature. Excess 1,1´-carbonyldiimidazole was decomposed through the addition of dry MeOH (0.3 mL, 6 mmol) and stirring for 1 h. This solution was added dropwise with mixing to a solution of the tributylammonium salt of pyrophosphate, (prepared from tetrasodium pyrophosphate) (2.0 g, 7.5 mmol) in dry DMF (10 mL). After reacting overnight at room temperature, the mixture was cooled to 0 °C in an ice bath. Cold water (15 mL, 4 °C) was added with mixing and then the pH was adjusted to 7 using 1 M NaOH. The reaction mixture was partitioned between diethyl ether and H_2O; the aqueous phase was evaporated with EtOH at 30 °C and dried. Crude product was purified by DEAE Sephadex A-25 column with the eluent of a linear gradient of 0.2-1.0 M TEAB solution (over 400 min) at 4 °C. The fractions were checked with ESI MS and the desired fractions were mixed with EtOH and evaporated. The resulting residue dried *in vacuo*. The obtained product was dissolved in dry MeOH (1 mL) upon addition of NaI in acetone (1 M, 10 mL) sodium salt of the product was precipitated. The precipitate was washed several times with acetone and lyophilized to afford 0.40 g (50 %) sodium salt of compound **1c** as a red powder. ^{1}H NMR (400 MHz, D_2O) δ 8.00 (dd, *J* = 7.9, 1.7 Hz, 2H), 7.71 – 7.54 (m, 6H), 7.46 (t, *J* = 8.4 Hz, 1H), 4.08 (q, *J* = 6.4 Hz, 2H), 3.27 (t, *J* = 7.8 Hz, 2H), 2.03 (quin, *J* = 7.1 Hz, 2H). ^{13}C

NMR (100 MHz, D_2O with some drops of CD_3OD as a standard) δ_C 153.25, 151.32, 141.91, 132.66, 132.62, 132.00, 130.54, 128.15, 123.57, 116.66, 67.13, 33.18, 28.16. ^{31}P NMR (160 MHz, D_2O (H_3PO_4 as external standard)) δ_P -9.72 (d, *J* = 19.5 Hz), -10.71 (d, *J* = 19.7 Hz), -22.84 (t, *J* = 19.4 Hz). HR-MS (ESI, *m*/*z*) calculated for $C_{15}H_{19}N_2O_{10}P_3$ $[M - H]^-$: 479.01798; found 479.01855.

2.4.4. Reverse-phase (RP) HPLC profile of 1c

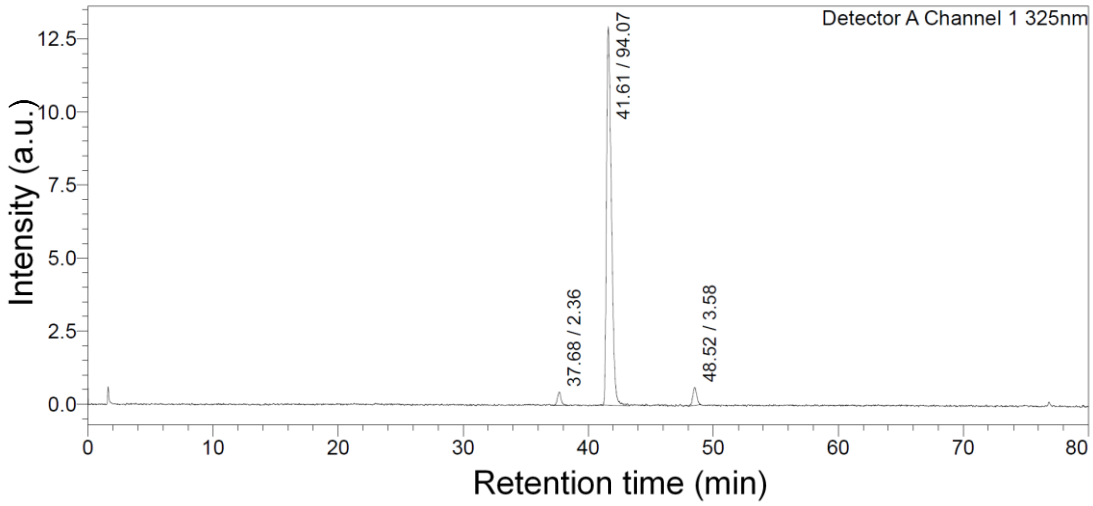

Fig. 2.15 RP HPLC chromatogram of **1c.** Retention time: 41.61 min (94%), Column: Mightysil, RP-18 GP (L) 150-4.6 (5μm) (Kanto Chemical). Eluent: 10–70 % of CH_3CN in sodium phosphate buffer (pH 6) for 80 min. Monitoring wavelength: 325 nm. Flow rate: 1.0 mL / min at room temperature.

2.4.5. Preparation of proteins

The kinesin used in this study was a recombinant kinesin consisting of 573 amino acid residues from the *N*-terminus of a conventional human kinesin. This recombinant kinesin, fused with His-tag at the *N*-terminus (plasmid; pET 30b), was expressed in *E*. *coli* Rossetta (DE3) pLysS and purified through the general method using Ni-NTA-agarose. Purified kinesin was distributed in small

aliquots and quickly frozen in liquid N_2 and stored at −80 °C until use. Tubulin was purified from porcine brains through two successive cycles of polymerization and depolymerization in the presence of a high-molarity PIPES buffer[16]. To prepare fluorescently labelled microtubules, tubulin was labelled with CF®633 Succinimidyl Ester (92133, Biotium). CF®633-microtubules were polymerized by copolymerizing labelled and unlabeled tubulin at a ratio 1:4 for 60 min at 37 °C and stabilized with paclitaxel.

Skeletal muscle myosin was purified from chicken pectoralis muscles and heavy meromyosin (HMM) was produced by digestion of myosin using α-chymotrypsin followed by dialysis[17]. The HMM was distributed in small aliquots and quickly frozen in liquid N_2 and stored at −80 °C until use. F-actin was extracted from acetone powder of rabbit skeletal muscle and prepared by partially modifying the previously reported method[18] and labelled with a phalloidin conjugated CF®633 dye (00046T, Biotium) at a 1/1.2 (actin/phalloidin) ratio. The fluorescently labelled actin was stored on ice for up to 4 weeks. Concentration of HMM and actin were determined from the absorbance at 280 nm using the extinction coefficients of 0.63 and 1.1 for 1 mg/ml solutions, respectively.

2.4.6. *In vitro* microtubule-kinesin gliding assay

Microtubule gliding on surface bound kinesin motors in a flow cell was observed using fluorescence microcopy at 25 °C, as described previously[1]. A flow chamber was first filled with 3.5 µL solution of kinesin (300 nM) with casein (0.5 mg/mL) in BRB-80 buffer (pH 6.9; PIPES, 80 mM; $MgCl_2$, 2 mM; EGTA, 1 mM) and incubated at room temperature for 3 min. Then paclitaxel stabilized microtubules (0.25 µM as tubulin dimer) in BRB-80 buffer containing paclitaxel (10 µM) and

casein (0.1 mg/mL) was perfused and incubated at room temperature for 3 min. After washing with 3.5 µL of BRB80 buffer containing paclitaxel (10 µM) and casein (0.1 mg/mL) incubated for 1 min. Then BRB80 buffer containing paclitaxel (10 µM), β-mercaptoethanol (0.14 M), glucose oxidase (0.1 mg/mL), catalase (20 µg/mL), glucose (20 mM), casein (0.5 mg/mL) and energy molecule (AzoTP derivatives, 0.05 - 2.0 mM) was perfused into the flow chamber. Then the flow cell was subjected to microtubules gliding motility observation under fluorescence microscope. Microtubule filaments gliding was imaged using epifluorescence microscope based on an IX 70 (Olympus) equipped with a 60×/NA 1.45 oil immersion objective lens (PlanApo, Olympus). Images obtained under fluorescence microscope were projected onto EMCCD camera (DL-604M-0EM-H1, Andor Technology). The camera was controlled by the andor solis software platform ver. 4.23.30008.0. The typical frame rate was 1 sec and observation duration were 40 - 120 sec depending on the faster/slower movement of the microtubules. The position of the microtubules was determined manually by mouse clicking on the tip of the filament in the Fiji image processing software package based on ImageJ and tracked typically first and last frame of the observation. The gliding velocity of at least 10 microtubules in randomly chosen microscopic fields were measured in each experiment. The velocity of each filament was determined by a linear least-squares fit, assuming that the filaments move in a straight line. To study *cis-trans* rich state AzoTP derivatives induced microtubules gliding velocity, the flow cell was irradiated with UV 365 nm (0.68 W/cm^2) light for 8 sec and visible 436 nm (21.7 mW/cm^2) light for 25 sec respectively.

2.4.7. *In vitro* actin-myosin gliding motility assay

Actin filaments gliding on nitrocellulose coated surface bound HMM motors in a flow cell was observed using fluorescence microcopy at 23.5 °C, as described previously[2]. In brief, 3.5 µL HMM (300 µg/ml) solution in assay buffer (pH 7.4; HEPES, 100 mM; $MgCl_2$, 4 mM; EGTA, 1 mM; NaCl, 25 mM; DTT, 10 mM) was added to flow chamber and incubated for 60 seconds. After 60 seconds, unbound HMM molecules were washed by 3.5 µL assay buffer with BSA (0.5 mg/ml) and incubate for 3 minutes. Then 3.5 µL of CF®633 phalloidin labelled actin (1.2 µg/ml) was perfused to the chamber and incubated for 60 seconds. After the incubation 3.5 µL solution of a scavenger cocktail [glucose oxidase (0.1 mg/mL), catalase (20 µg/mL), glucose (20 mM)], BSA (0.5 mg/ml) and AzoTPs/NTPs (0.05 - 2.0 mM) in assay buffer was perfused to the follow cell. Then the flow cell was subjected to actin filaments gliding motility observation under epifluorescence microscope (IX 70, Olympus) equipped with EMCCD camera (DL-604M-0EM-H1, Andor Technology). The typical frame rate was 0.5 sec and observation duration were 10 - 120 sec depending on the faster/slower movement of the actin filaments. The gliding velocity of at least 10 actin filaments in randomly chosen microscopic fields were measured in each experiment; however, stationary filaments that did not moved at all were excluded from velocity measurements. The gliding velocities were measured using MTrackJ plugin in the Fiji image processing software package based on ImageJ, typically each actin filament was tracked every 0.5 sec or 10 sec depending on the faster/slower movement of actin filaments.

2.4.8. Computational docking simulation

The computational docking simulation was carried out with the program of CLC Drug Discovery Workbench (QIAGEN, Denmark) using the parameters and scoring function of PLANTS(PLP) score[49]. We manually inspected with the docking modes with high-scored results.

2.4.9. Kinesin-myosin composite motility assay

The flow cell chamber for microscopic observation was prepared by taping a nitrocellulose coated cover slip (18 × 18 mm) and a glass slide (76 × 26 mm) together with the double-sided tape to make a flow path having a volume of 3 - 3.5 µL with a height of *ca*. 100 µm. The photocontrollable study was performed by direct irradiation of UV (365 nm, 0.68 W/cm^2) and visible (436 nm, 21.7 mW/cm^2) light to the flow chamber. To achieve the kinesin-myosin composite motility assay, the perfusion protocol shown below was followed, 3.5 µL HMM (300 µg/mL) solution in assay buffer (pH 7.4; HEPES, 100 mM; $MgCl_2$, 4 mM; EGTA, 1 mM; NaCl, 25 mM; DTT, 1 mM) was added to the flow chamber and it was incubated for 60 seconds. After 60 seconds, 3.5 µL of kinesin solution containing BSA (kinesin: ca. 300 nM; BSA: 5.0 mg/mL) in the assay buffer was perfused into the chamber and it was also incubated for 3 min. Next, 3.5 µL solution of fluorescent dye labelled microtubules (0.25 µM as tubulin dimer) containing paclitaxel (10 µM) and BSA (0.5 mg/mL) in the assay buffer was perfused to the chamber and it was incubated for 60 seconds. Then, 3.5 µL of fluorescent dye labelled actin (1.2 µg/ml) containing paclitaxel (10 µM) and BSA (0.5 mg/mL) in assay buffer was perfused to the chamber and it was incubated for 60 seconds. After the incubation, 3.5 µL solution of a scavenger mixture

[paclitaxel (10 μM), glucose oxidase (0.1 mg/mL), catalase (20 μg/mL), glucose (20 mM)], BSA (0.5 mg/ml), **1e**/ATP (desired concentration)] in the assay buffer was perfused to the follow cell. The flow cell was subjected to microtubules and actin filaments motility observation under epifluorescence microscope (IX 70, Olympus) equipped with EMCCD camera (DL-604M-0EM-H1, Andor Technology) at 25 °C.

2.5. References and notes

1 N. Perur, M. Yahara, T. Kamei and N. Tamaoki, *Chem. Commun.*, 2013, **49**, 9935–9937.

2 H. M. Menezes, M. J. Islam, M. Takahashi and N. Tamaoki, *Org. Biomol. Chem.*, 2017, **15**, 8894–8903.

3 F. Jon Kull, E. P. Sablin, R. Lau, R. J. Fletterick and R. D. Vale, *Nature*, 1996, **380**, 550–555.

4 A. Weber, *J. Gen. Physiol.*, 1969, **53**, 781-791.

5 S. A. Cohn, A. L. Ingold and J. M. Scholey, *J. Biol. Chem.*, 1989, **264**, 4290–4297.

6 T. Shimizu, K. Furusawa, S. Ohashi, Y. Y. Toyoshima, M. Okuno, F. Malik and R. D. Vale, *J. Cell Biol.*, 1991, **112**, 1189–1197.

7 H. D. White, B. Belknap and W. Jiang, *J. Biol. Chem.*, 1993, **268**, 10039–10045.

8 E. Pate, K. Franks-Skiba, H. White and R. Cooke, *J. Biol. Chem.*, 1993, **268**, 10046–10053.

9 S. Higashi-Fujime and T. Hozumi, *Biochem. Biophys. Res. Commun.*, 1996, **221**, 773–778.

10 S. M. Frisbie, J. M. Chalovich, B. Brenner and L. C. Yu, *Biophys. J.*, 1997, **72**, 2255–2261.

11 M. Regnier, D. M. Lee and E. Homsher, *Biophys. J.*, 1998, **74**, 3044–3058.

12 M. Regnier and E. Homsher, *Biophys. J.*, 1998, **74**, 3059–3071.

13 I. Amitani, T. Sakamoto and T. Ando, *Biophys. J.*, 2001, **80**, 379–397.

14 L. Farhadi, C. F. Do Rosario, E. P. Debold, A. Baskaran and J. L. Ross, *Front*.

Phys., 2018, **6**, 75.

15 Usually at higher concentration of AzoTPs (> 3.5 mM), the microtubules were detached form kinesin and floating in the flow cell. In case of **1e**, the detachment of microtubules was observed at >2.0 mM concentration. Therefore, the microtubule gliding velocity was shown up to 3.0 mM for all AzoTP derivatives except for **1e** (up to 2.0 mM).

16 M. Castoldi and A. V. Popov, *Protein Expr. Purif.*, 2003, **32**, 83–88.

17 S. S. Margossian and S. Lowey, *Methods Enzymol*., 1982, **85**, 55–71.

18 J. D. Pardee and J. A. Spudich, *Methods Enzymol*., 1982, **85**, 164–181.

19 O. Knob, T. Stutzle and T. E. Exner, *J. Chem. Inf. Model.*, 2009, **49**, 84-96

Chapter 3.

Non-hydrolysable azo-triphospahte molecules as photo-responsive inhibitor for myosin and kinesin motor proteins

3.1. Introduction

Substrate analogs which resemble the natural substrate sufficiently well to interact with the active site of an enzyme can provide important new insights into mechanism. The β, γ-Imidoadenosine 5′-triphosphate (AMP-PNP) and β, γ-Methyleneadenosine 5'-triphosphate (AMP-PCP), the non-hydrolysable ATP analogs, where the oxygen atom bridging the β to the γ phosphate is replaced by a nitrogen or carbon atom respectively. The AMP-PNP and AzoMP-PCP were well known ATPase inhibitor for many ATPase including motor protein ATPase[1,2].

Since the photo-reversible energy molecule AzoTPs were enzyme substrate for both kinesin and myosin bio-molecular motors where the enzyme activity could be reversibly switched by *cis-trans* isomerization of azobenzene[3,4].

Herein, the author explores the inhibitory behavior of AzoTP **1a**, **1b** and **1e** based several non-hydrolysable tri-phosphate molecules in the actin-myosin and microtubules-kinesin *in vitro* motility assay. The non-hydrolysable tri-phosphate molecule **2a**, the oxygen atom bridging the β to the γ phosphate is replaced by a nitrogen, showed inhibitory activity with photo-reversible manner in both myosin and kinesin motor protein systems.

3.2. Results and discussion

3.2.1. Synthesis and photoisomerization of non-hydrolysable azo-triphosphate molecules

To explore the photo-responsive inhibitory activities of non-hydrolysable derivatives of AzoTPs towards myosin and kinesin, the author synthesized four non-hydrolysable derivatives of AzoTP, **2a**-**2d** (Fig 3.1).

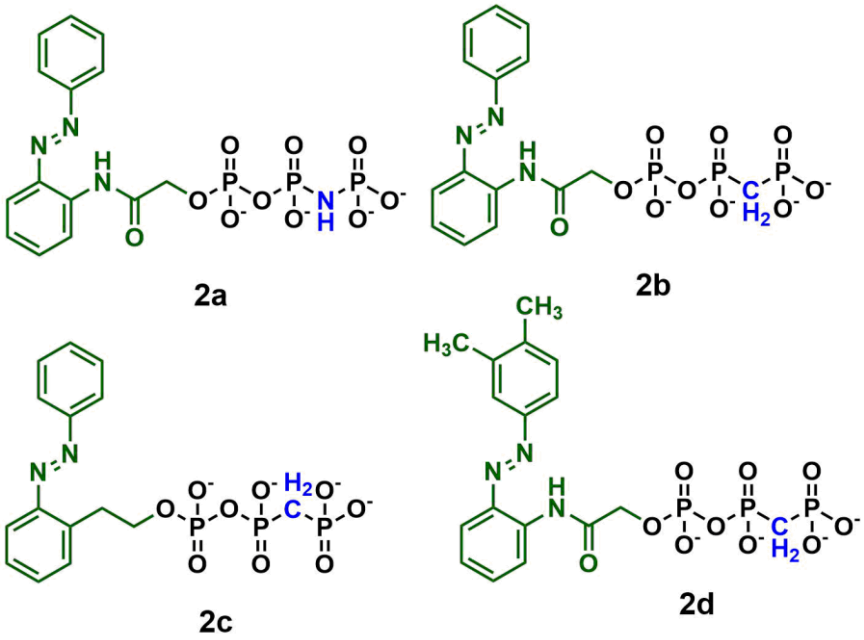

Fig. 3.1 Structure of non-hydrolysable azo-triphosphate inhibitors, **2a**-**2d**

The non-hydrolysable azo-triphosphate molecules, **2a** and **2b** were designed based on AzoTP **1a** where the -o- bridge in the β-γ phosphate bond of the triphosphate was replaced with -NH- and -CH_2- bridge respectively. Similarly, **2c** and **2d** were designed based on AzoTP **1b** and **1e** respectively, replacing the -o- bridge with -CH_2-. The synthesis route of non-hydrolysable azo-triphosphate molecules involve multi step synthesis similar to AzoTP molecules with modification in the last step where targeted azo-triphosphate was obtained coupling between azo-monophosphate and pyrophosphate. The detail of the synthesis and characterization were shown in materials and method section.

Since the non-hydrolysable azo-triphosphate molecules contain same azobenzene chromophore like AzoTPs, the author expected similar reversible photoisomerization behavior with ultraviolet (UV) and visible (VIS) light irradiation. UV-VIS spectra of **2a**-**2d** in BRB-80 buffer before irradiation (BI) and after UV (365 nm) or VIS (436 nm) irradiation were shown in Fig. 3.2.

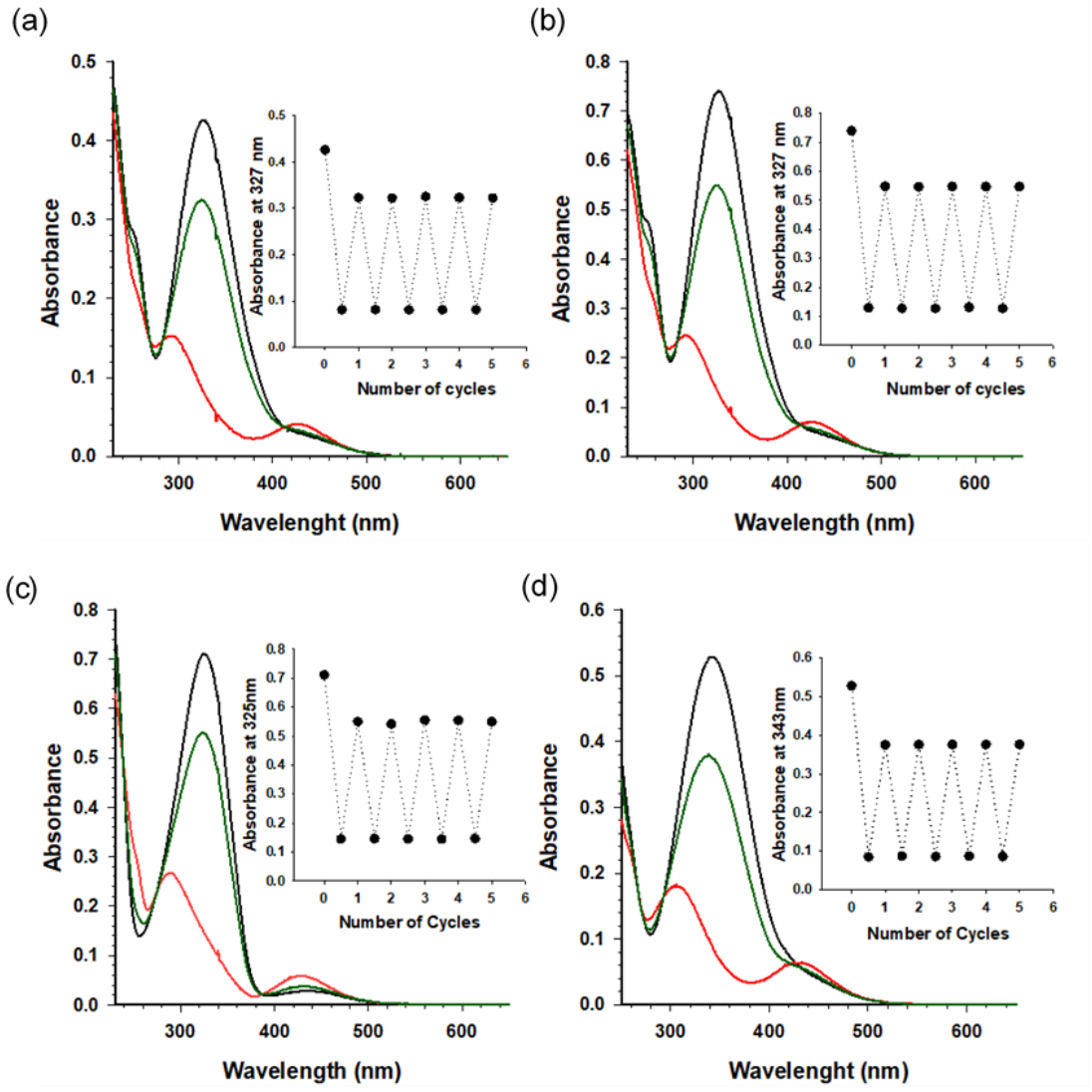

Fig. 3.2 UV-VIS absorption spectra of **2a**-**2d** before irradiation and at UV photo stationary state (PSS) and VIS PSS. UV-VIS absorption spectra of (a) **2a** (2.7×10^{-4} M), (b) **2b** (4.6×10^{-4} M), (c) **2c** (5.0×10^{-4} M) and (d) **2d** (4.6×10^{-4} M) in BRB-80 buffer at 25 °C. Before irradiation (black line), UV PSS (red line), VIS

PSS (dark green line). Insets: Absorbance changes after the alternate irradiations with UV (20 sec) and VIS (150 sec) light for 5 cycles.

The non-hydrolysable azo-triphosphate **2a**-**2e** showed reversible photoisomerization by irradiation with UV and VIS light reversibly. The reversible photoisomerization of could be recycled several times by alternating UV and VIS light irradiation without any fatigues.

3.2.2. Non-hydrolysable azo-triphosphate molecules in actin-myosin in vitro motility assay

After confirming the reversible photoisomerization behavior of non-hydrolysable azo-triphosphate molecules, the author applied the **2a**-**2d** (3.0 mM) in actin-myosin in-vitro motility assay with ATP (0.50 mM). The author measured the actin filaments gliding motility at BI, after UV and after VIS light irradiation. Gliding velocities of actin filaments without and with **2a**-**2d** at different light irradiation condition were shown in Fig. 3.3. In the *trans* state (BI) of **2a**-**2d,** the gliding velocity was decreased 41%-74% of the original velocity with ATP, in the cis-rich state, obtain after irradiation with UV light, the gliding velocity was increased. These gliding velocities changed reversibly by alternate irradiation with UV and VIS light. Table 3.1 summarizes the inhibitory behavior of non-hydrolysable azo-triphosphate molecules in actin-myosin *in vitro* motility assay. The azo-triphosphate, **2a** showed highest 74% gliding velocity inhibition at BI (*trans* state) while the **2b** showed 41% gliding velocity inhibition. In case of gliding velocity recovery after UV irradiation (cis-rich state) the 2d showed almost 99% initial velocity recovery (1.2% inhibition).

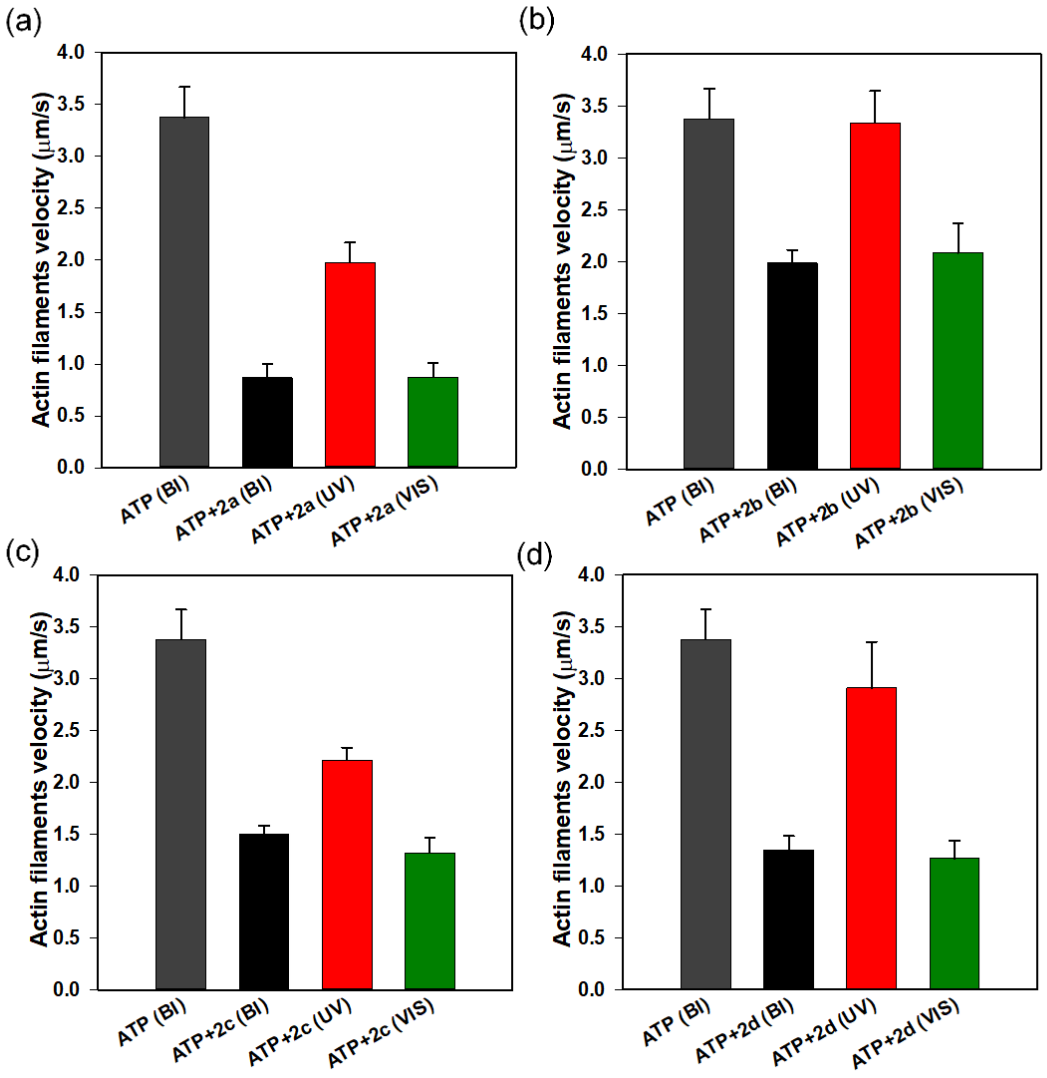

Fig 3.3 Actin filaments gliding velocity without or with non-hydrolysable azo-triphosphate molecules (a) **2a**, (b) **2b**, (c) **2c** and (d) **2d** at different light irradiation condition (concentration of ATP = 0.50 mM and **2a**-**2d** = 3.0 mM). Error bars represent the standard deviation of 10 actin filaments in a single flow cell.

Table 3.1 Inhibitory behavior of non-hydrolysable azo-triphosphate molecules in actin-myosin motility assay

Inhibitor molecules	Gliding velocity inhibition* (%)	
	BI	UV
2a	74	41
2b	41	1.2
2c	56	34
2d	60	14

*Concentration of ATP = 0.50 mM and **2a**-**2d** = 3.0 mM

3.2.3. Non-hydrolysable azo-triphosphate molecules in microtubule-kinesin in vitro motility assay

Encouraged by the non-hydrolysable azo-triphosphate molecule's photo-responsive inhibitory behavior in actin-myosin *in vitro* motility assay, the author investigated the non-hydrolysable azo-triphosphate molecules in microtubule-kinesin motility assay. The author explored **2a**, showed the maximum inhibition effect in actin-myosin system (at BI), and **2d**, the corresponding original energy molecule showed myosin specificity. The author measured the microtubules gliding motility at BI, and after UV light irradiation. Gliding velocities of microtubules without and with **2a** or **2d** at different light irradiation condition were shown in Fig. 3.4. In the *trans* state (BI)**,** the gliding velocity was decreased 41% of the original velocity of ATP with **2a**, while **2d** showed only 10% decrement of the original velocity of ATP. In the cis-rich state, obtain after irradiation with UV light, the gliding velocity with **2a** was increased to 89% (11% gliding velocity

inhibition) of the initial velocity of ATP. In the case of **2d**, the gliding velocity switching was negligible (BI = 0.50 ±0.06 µm/s and UV = 0.48 ± 0.04).

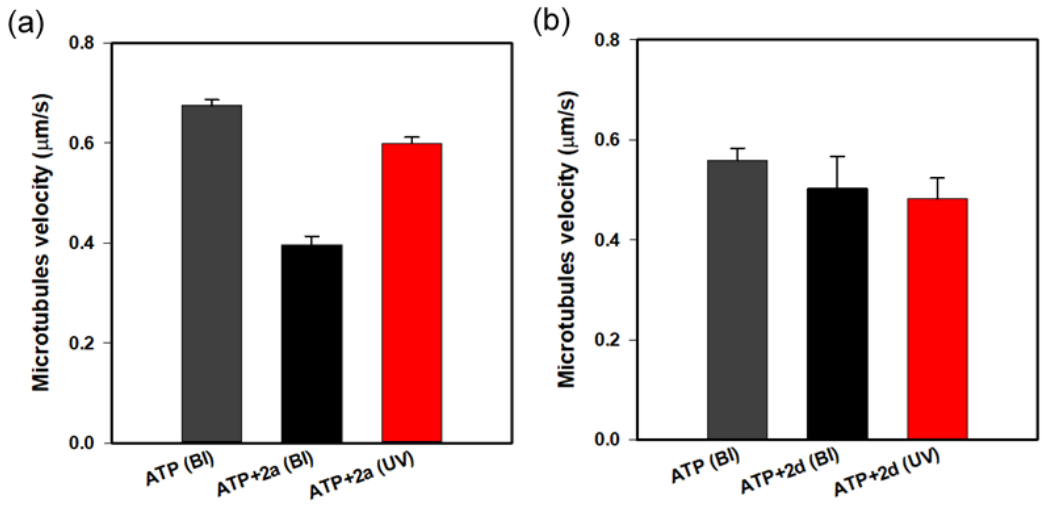

Fig 3.4 Microtubule gliding velocity without or with non-hydrolysable azo-triphosphate molecules (a) **2a** (concentration of ATP = 0.30 mM and **2a** = 3.0 mM) and (b) **2d** (concentration of ATP = 1.0 mM and **2a** = 2.0 mM) at different light irradiation condition. Error bars represent the standard deviation of 10 microtubules in a single flow cell.

Table 3.2 Inhibitory behavior of non-hydrolysable azo-triphosphate molecules in microtubule-kinesin motility assay

Inhibitor molecules	Gliding velocity inhibition* (%)	
	BI	UV
2a	41	11
2d	10	14

Table 3.2 summarizes the inhibitory behavior of **2a** and **2d** in microtubule-kinesin *in vitro* motility assay. These results indicated that the non-hydrolysable azo-triphosphate **2d** had negligible inhibition effect in microtubule-kinesin motility assay. Which relate the bulky two methyl group substitution on azobenzene moiety hindered the recognition in kinesin active site.

3.3. Conclusion

The non-hydrolysable azo-triphosphate molecules especially **2a** works as photo-responsive inhibitor for actin-myosin and microtubule-kinesin both motor system. The non-hydrolysable azo-triphosphate molecule **2d** had specificity towards actin-myosin motor system as photo-responsive inhibitor. These reversible inhibitory activities of non-hydrolysable azo-triphosphate molecules could be well explained by reversible change in affinity of the azo-triphosphate molecules to motor proteins upon photo isomerization.

3.4. Materials and methods

3.4.1. Synthesis of non-hydrolysable azo-triphosphate molecules

The general synthesis route was similar to AzoTP molecules except in the last step where monophosphate was coupling with pyrophosphate to from the targeted AzoTP molecules. Therefore the author depicted the last step of the synthesis in scheme 3.1.

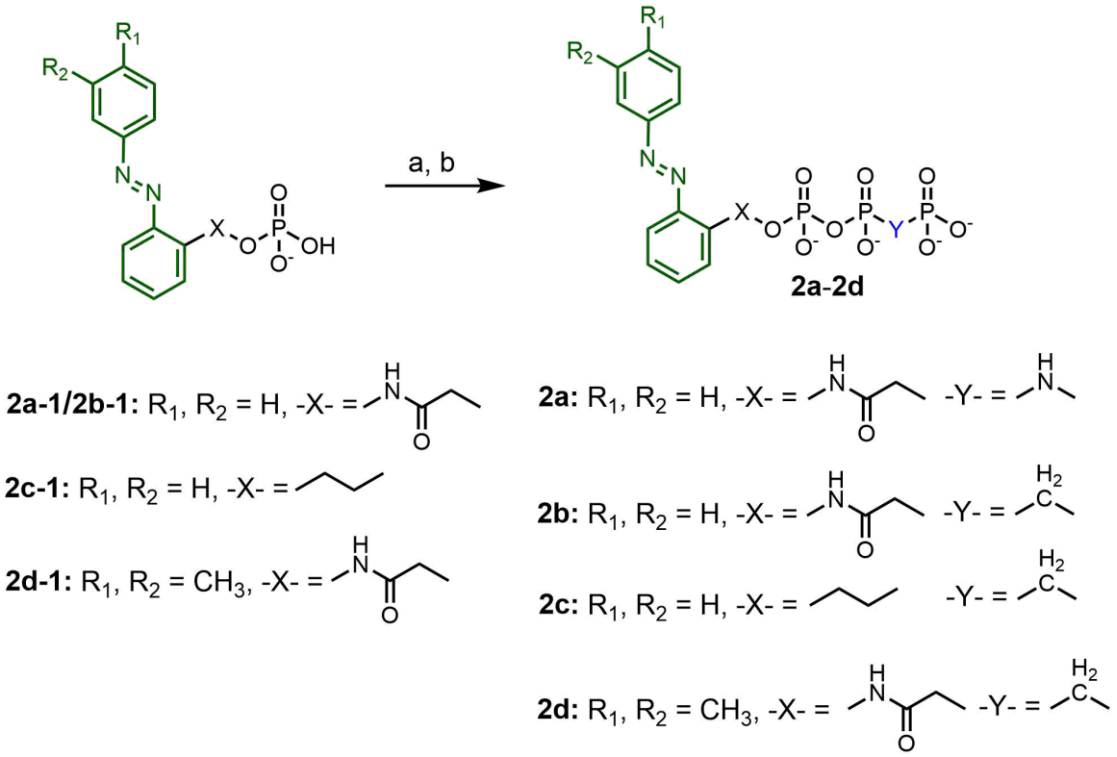

Scheme 3.1 Synthetic scheme of **2a**-**2d**. Reagent and condition: (a) Tributylamine, carbonyldiimidazole, Ar-atmosphere, RT, 16h (b) Tributylammonium-imidodiphosphate (for **2a**) or tributylammonium-methylenediphosphate (for **2b**-**2d**), dry DMF, Ar-atmosphere, RT, overnight.

Non-hydrolysable azo-triphosphate 2a:

Triethyl ammonium salt of **2a-1** (0.71g, 1.3 mmol) was converted in its tributylammonium salt through addition of tributylamine (1.0 mL) in dry MeOH (7.0 mL). Triethylamine and MeOH were removed through *rotovap*. The tributylammonium salt was dissolved in dry DMF (6.0 mL). While stirring, a solution of 1,1´-carbonyldiimidazole (1.2 g, 7.5 mmol) in dry DMF (5 mL) was added under Ar-atmosphere and then the reaction was left for 16 h at room temperature. Excess 1,1´-carbonyldiimidazole was destroyed through the addition of dry MeOH (0.3 mL, 6 mmol) and stirring for 1 h. This solution was

added dropwise with mixing to a solution of the tributylammonium salt of imidodiphosphate, (prepared from imidodiphosphate sodium salt, 1.0 g, 3.8 mmol) in dry DMF (10 mL). After reacting overnight at room temperature, the mixture was cooled to 0 °C in an ice bath. Cold water (15 mL, 4 °C) was added with mixing and then the pH was brought to 7.5 using 1 M NaOH. The reaction mixture was partitioned between ether and H_2O; the aqueous phase was evaporated with EtOH at 30 °C and dried. Crude product was purified by DEAE Sephadex A-25 column. The compound was eluted using a linear gradient of 0.2-1.0 M TEAB solution at 4 °C. The fractions containing the product as confirmed using ESI MS were mix with EtOH and evaporated using a *rotovap* and the residue dried under vacuum. The obtained product was dissolved in dry MeOH (1mL) upon addition of NaI in acetone (1M, 10mL) sodium salt of the product was precipitated. The precipitated was washed several times with acetone and dried by lyophilizer to afford 55 g (7.3%) of Compound **2a** as sodium salt. ^{1}H NMR (400 MHz, D_2O) δ 7.97 – 7.94 (m, 2H), 7.90 (dd, *J* = 8.1, 1.1 Hz, 1H), 7.73 (dd, *J* = 8.2, 1.4 Hz, 1H), 7.67 – 7.62 (m, 4H), 7.49 – 7.35 (m, 1H), 4.67 (d, *J* = 7.3 Hz, 2H).

Non-hydrolysable azo-triphosphate 2b:

Triethyl ammonium salt of **2b-1** (0.28g, 0.52 mmol) was converted in its tributylammonium salt through addition of tributylamine (0.8 mL) in dry MeOH (6.0 mL). Triethylamine and MeOH were removed through *rotovap*. The tributylammonium salt was dissolved in dry DMF (6.0 mL). While stirring, a solution of 1,1´-carbonyldiimidazole (0.52 g, 3.25 mmol) in dry DMF (5 mL) was added under Ar-atmosphere and then the reaction was left for 16 h at room temperature. Excess 1,1´-carbonyldiimidazole was destroyed through the

addition of dry MeOH (0.136 mL, 2.72 mmol) and stirring for 1 h. This solution was added dropwise with mixing to a solution of the tributylammonium salt of methylenediphosphonic acid, (prepared from methylenediphosphonic acid) (0.62 g, 3.5 mmol) in dry DMF (5 mL). After reacting overnight at room temperature, the mixture was cooled to 0 °C in an ice bath. Cold water (15 mL, 4 °C) was added with mixing and then the pH was brought to 7.5 using 1 M NaOH. The reaction mixture was partitioned between ether and H_2O; the aqueous phase was evaporated with EtOH at 30 °C and dried. Crude product was purified by DEAE Sephadex A-25 column. The compound was eluted using a linear gradient of 0.2-1.0 M TEAB solution at 4 °C. The fractions containing the product as confirmed using ESI MS were mix with EtOH and evaporated using a *rotovap* and the residue dried under vacuum. The obtained product was dissolved in dry MeOH (1mL) upon addition of NaI in acetone (1M, 10mL) sodium salt of the product was precipitated. The precipitated was washed several times with acetone and dried by lyophilizer to afford 0.188 g (62%) of Compound **2b** as sodium salt. ^{1}H NMR (400 MHz, D_2O) δ 8.02 (dd, *J* = 8.2, 1.0 Hz, 1H), 7.94 – 7.92 (m, 2H), 7.70 (dd, *J* = 8.1, 1.3 Hz, 1H), 7.64 – 7.58 (m, 4H), 7.41 – 7.37 (m, 1H), 4.65 (d, *J* = 7.2 Hz, 2H), 2.39 (t, *J* = 20.6 Hz, 2H).

Non-hydrolysable azo-triphosphate 2c:

Triethyl ammonium salt of **2c-1** (0.20g, 0.5 mmol) was converted in its tributylammonium salt through addition of tributylamine (1.0 mL) in dry MeOH (6.0 mL). Triethylamine and MeOH were removed through *rotovap*. The tributylammonium salt was dissolved in dry DMF (6.0 mL). While stirring, a solution of 1,1´-carbonyldiimidazole (0.36 g, 2.2 mmol) in dry DMF (3 mL) was added under Ar-atmosphere and then the reaction was left for 16 h at room

temperature. Excess 1,1´-carbonyldiimidazole was destroyed through the addition of dry MeOH (70 µL) and stirring for 1 h. This solution was added dropwise with mixing to a solution of the tributylammonium salt of methylenediphosphonic acid, (prepared from methylenediphosphonic acid, 0.55 g, 3.1 mmol) in dry DMF (5 mL). After reacting overnight at room temperature, the mixture was cooled to 0 °C in an ice bath. Cold water (15 mL, 4 °C) was added with mixing and then the pH was brought to 7.5 using 1 M NaOH. The reaction mixture was partitioned between ether and H_2O; the aqueous phase was evaporated with EtOH at 30 °C and dried. Crude product was purified by DEAE Sephadex A-25 column. The compound was eluted using a linear gradient of 0.2-1.0 M TEAB solution at 4 °C. The fractions containing the product as confirmed using ESI MS were mix with EtOH and evaporated using a *rotovap* and the residue dried under vacuum. The obtained product was dissolved in dry MeOH (1mL) upon addition of NaI in acetone (1M, 10mL) sodium salt of the product was precipitated. The precipitated was washed several times with acetone and dried by lyophilizer to afford 0.185 g (67%) of Compound **2c** as sodium salt. ^{1}H NMR (400 MHz, D_2O) δ 7.94 (dd, *J* = 7.9, 1.8 Hz, 2H), 7.64 – 7.51 (m, 6H), 7.44 – 7.40 (m, 1H), 4.21 (dd, *J* = 14.5, 7.0 Hz, 2H), 3.47 (t, *J* = 6.8 Hz, 2H). 2.31 (t, *J* = 20.6 Hz, 2H). ESI-MS (ESI$^-$, *m*/*z*) calculated for $C_{15}H_{17}N_2NaO_9P_3^-$ [M - H]$^-$: 485.01.; found 485.07.

Non-hydrolysable azo-triphosphate 2d:

The triethylammonium salt of compound **2d-1** (0.37g, 0.79 mmol) was converted to its tributylammonium salt through the addition of tributylamine (0.75 mL, 3 mmol) in dry MeOH (5 mL). Triethylamine and MeOH were removed through *rotovap*. The tributylammonium salt was dissolved in dry DMF (8 mL). While

stirring, a solution of 1,1´-carbonyldiimidazole (0.61 g, 3.76 mmol) in dry DMF (5 mL) was added under Ar-atmosphere and then the reaction was left for 16 h at room temperature. Excess 1,1´-carbonyldiimidazole was destroyed through the addition of dry MeOH (0.12 mL, 2.96 mmol) and stirring for 1 h. This solution was added dropwise with mixing to a solution of the tributylammonium salt of methylenediphosphonic acid, (prepared from methylenediphosphonic acid, 0.62 g, 3.5 mmol) in dry DMF (5 mL). After reacting overnight at room temperature, the mixture was cooled to 0 °C in an ice bath. Cold water (15 mL, 4 °C) was added with mixing and then the pH was brought to 7.5 using 1 M NaOH. The reaction mixture was partitioned between ether and H_2O; the aqueous phase was coevaporated with EtOH at 30 °C and dried in a *rotovap*. Crude product was purified by DEAE Sephadex A-25 column. The compound was eluted using a linear gradient of 0.2-1.0 M TEAB solution at 4 °C. The fractions containing the product as confirmed using ESI MS were coevaporated with EtOH by using a *rotovap* and the residue was dried under vacuum. The obtained product was dissolved in dry MeOH (1mL) upon addition of NaI in acetone (1M, 10mL) sodium salt of the product was precipitated. The precipitated was washed several times with acetone and dried by lyophilizer to afford 0.39 g (81%) of Compound **2d** as sodium salt. ^{1}H NMR (400 MHz, D_2O) δ 7.99 (dd, *J* = 8.1, 0.9 Hz, 1H), 7.65 – 7.62 (m, 3H), 7.59 – 7.55 (m, 1H), 7.41 – 7.35 (m, 2H), 4.64 (d, *J* = 7.2 Hz, 2H), 2.38 (t, *J* = 20.6 Hz, 2H), 2.33 (d, *J* = 8.2 Hz, 6H). ESI-MS (ESI^-, *m*/*z*) calculated for $C_{17}H_{21}N_3O_{10}P_3^-$ $[M - H]^-$: 520.04.; found 520.20

3.4.2. Preparation of proteins

The kinesin, tubulin (microtubule), myosin and actin used in this study was same as described previously (Section 2.4.5).

3.4.3. *In vitro* actin-myosin gliding assay

Actin filaments gliding on surface bound myosin motors in a flow cell was observed using fluorescence microcopy at 23.5 °C, as described previously (Section 2.4.7)

3.4.4. *In vitro* microtubule-kinesin gliding assay

Microtubule gliding on surface bound kinesin motors in a flow cell was observed using fluorescence microcopy at 23.5 °C, as described previously (Section 2.4.6)

3.5 References

1 R. G. Yount, D. Ojala and D. Babcock, *Biochemistry*, 1971, **10**, 2490–2496.

2 H. S. Penefsky, *Chem. Commun.*, 1974, **249**, 3579–3585.

3 N. Perur, M. Yahara, T. Kamei and N. Tamaoki, *Chem. Commun.*, 2013, **49**, 9935–9937.

4 H. M. Menezes, M. J. Islam, M. Takahashi and N. Tamaoki, *Org. Biomol. Chem.*, 2017, **15**, 8894–8903.

Chapter 4.

Conclusions of the thesis

In this dissertation work, the author discovered myosin-selective photo-responsive energy molecule, AzoTP **1e** by studying the powering activity of several AzoTP molecules in the microtubule-kinesin and actin-myosin motility assay respectively. This myosin selectivity of **1e** was explained by its binding modes with kinesin or myosin motors through the docking simulation study. Moreover, the author has demonstrated selective and reversible photoregulation of myosin motility using **1e** in kinesin-myosin composite motility assay, where both kinesin and myosin were attached on the same glass surface and microtubules and actin filaments were glided over the motor proteins.

Further the author explored the photoresponsive inhibitory behavior several non-hydrolysable azo-triphosphate molecules in kinesin and myosin motor protein system. The non-hydrolysable azo-triphosphate molecule especially **2a**, which was designed based on AzoTP **1a** works as photo-responsive inhibitor for kinesin and myosin motor protein system. On the other hand, the **2d**, which was designed based on AzoTP **1e** showed effective photo-responsive inhibitory behavior on myosin motor system. Which implies the bulky dimethyl substitution on azobenzene moiety impeded the kinesin substrate recognition.

The author envisions that the motor-specific AzoTP can be a chemical tool for unveiling the motor-based biological processes and constructing nanotechnological system using the microtubule and actin composite system.

List of publication

(1) “Substrate selectivity and its mechanistic insight of the photo-responsive non-nucleoside triphosphate for myosin and kinesin”

Md. Jahirul Islam, Kazuya Matsuo, Halley M. Menezes, Masayuki Takahashi, Hidehiko Nakagawa, Akira Kakugo, Kazuki Sada and Nobuyuki Tamaoki,

Org. Biomol. Chem., **2019**, 17, 53-65.

(2) “Driving and photo-regulation of myosin–actin motors at molecular and macroscopic levels by photo-responsive high energy molecules”

Halley M. Menezes, Md. Jahirul Islam, Masayuki Takahashi and Nobuyuki Tamaoki,

Org. Biomol. Chem., 2017, 15, 8894-8903.

(3) Selective and reversible photoregulation of kinesin and myosin motor proteins

Md. Jahirul Islam, Nobuyuki Tamaoki (Manuscript under preparation).

(4) Non-hydrolysable azo-triphospahte as photo-responsive inhibitor for kinesin and myosin motor proteins

Md. Jahirul Islam, Nobuyuki Tamaoki (Manuscript under preparation).

Acknowledgements

The author would like expresses his sincere gratitude and thank to his supervisor Professor Nobuyuki Tamaoki for his guidance, inspiration, and continuous support throughout the doctoral research.

The author also would like to thank Professor Masayuki Takahashi (Hokkaido University) for his valuable guidance and help during the myosin and actin protein preparation. The author also thanks Professor Akira Kakugo and Professor Kazuki Sada (Hokkaido University) for their support and help during kinesin and tubulin preparation. The author also would like to thank Professor Hidehiko Nakagawa (Nagoya City University) for helping the docking simulation study.

The author would like to thank all former and current members of the Professor Tamaoki lab (2013-2018), Dr. Nishad Perur, Dr. Rijeesh K Nair, Dr. Sunil Kumar K. R., Dr. Rika Ochi, Dr. Halley M. M., Dr. A., S., Amrutha, Ms. Mariko Ooki, Ms. Hiroko Tayyama, Mr. Nakamoto Y, Mr. Ito S., Mr. Yoshida K., Mr. Viswanata H. M., Mr. Furuta R., Mr. Ashino F., Ms. N., N., Mafy, Mr. Sampreeth T., Mr. Shariful Haque, Mr. T., Muramatsu, Mr. K., Ueda and Mr. Qi Jiajun, Mr. Lin Runze. The author gratefully acknowledges Assistant Professors, Dr. Yoshimitsu Sagara, Dr. Yuna Kim in Professor Tamaoki lab for their warm suggestion and helpful discussion. The author sincerely thanks to Assistant Professor Dr. Kazuya Matsuo in Professor Tamaoki lab for the docking simulation study and his generous support and help in the manuscript writing process.

The author acknowledges the program organizers of IGP-RPLS. The author thanks all his friends for helpful and hearty support.

The author was financial supported by IGP-RPLS (MEXT) scholarship.